

**EXPERIMENTAL ASSESSMENT OF MECHANICAL
AND HYDRAULIC PERFORMANCE OF FLY ASH-
MIXED-CEMENT GROUTS IN ROCK FRACTURES**



**A Thesis Submitted in Partial Fulfillment of the Requirements for the
Degree of Master of Engineering in Geotechnology
Suranaree University of Technology
Academic Year 2016**

การทดสอบศักยภาพเชิงกลศาสตร์และพลศาสตร์ของถ່วนผสมเถ้าลอยซีเมนต์
เพื่ออุดรอยแตกในหิน



วิทยานิพนธ์นี้เป็นส่วนหนึ่งของการศึกษาตามหลักสูตรปริญญาวิศวกรรมศาสตรมหาบัณฑิต
สาขาวิชาเทคโนโลยีธรณี
มหาวิทยาลัยเทคโนโลยีสุรนารี
ปีการศึกษา 2559

**EXPERIMENTAL ASSESSMENT OF MECHANICAL AND
HYDRAULIC PERFORMANCE OF FLY ASH-MIXED-CEMENT
GROUTS IN ROCK FRACTURES**

Suranaree University of Technology has approved this thesis submitted in partial fulfillment of the requirements for a Master's Degree.

Thesis Examining Committee



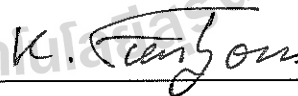
(Assoc Prof. Dr. Pornkasem Jongpradist)

Chairperson



(Dr. Prachya Tepnarong)

Member (Thesis Advisor)



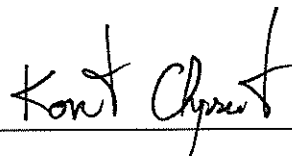
(Prof. Dr. Kittitep Fuenkajorn)

Member



(Prof. Dr. Sukit Limpijumnong)

Vice Rector for Academic Affairs
and Innovation



(Assoc. Prof. Ft. Lt. Dr. Kontorn Chamniprasart)

Dean of Institute of Engineering

มณฑล เชียงใหม่ : การทดสอบศักยภาพเชิงกลศาสตร์และชลศาสตร์ของส่วนผสมเถ้าลอย
ซีเมนต์เพื่ออุดรอยแตกในหิน (EXPERIMENT ASSESSMENT OF MECHANICAL
AND HYDRAULIC PERFORMANCE OF FLY ASH-MIXED-CEMENT GROUTS IN
ROCK FRACTURES) อาจารย์ที่ปรึกษา : อาจารย์ ดร.ปรัชญา เทพนรงค์, 107 หน้า.

วัตถุประสงค์ของการศึกษานี้เพื่อประเมินศักยภาพของเถ้าลอยกับปูนซีเมนต์ปอร์ตแลนด์
ประเภท 1 เพื่อใช้ลดความซึมผ่านของน้ำในรอยแตกของหินทราย ซึ่งรอยแตกถูกทำขึ้นโดยแรงกด
ในแนวเส้นบนตัวอย่างหินทรายชุดภูกระดึงเพื่อให้หินแตกออกจากกันด้วยแรงดึง เถ้าลอยจาก
โรงไฟฟ้าแม่เมาะถูกนำมาทดสอบคุณสมบัติเชิงกายภาพและเชิงเคมี การหาค่าความหนืดที่น้อยสุด
ของส่วนผสมที่ให้ค่ากำลังที่เหมาะสม สัดส่วนของเถ้าลอยต่อซีเมนต์และน้ำ (F:C:W) ที่ใช้ใน
การศึกษาเท่ากับ 1:10:10, 3:10:10, และ 5:10:10 และสัดส่วนเบนทอนไนต์ต่อซีเมนต์และน้ำ
(B:C:W) เท่ากับ 1:10:10, 2:10:10, และ 3:10:10 โดยน้ำหนัก ซึ่งส่วนผสมดังกล่าวให้ค่าความหนืด
ของส่วนผสมเหลวไม่ต่ำกว่า 5 ปาสคาล·วินาที และที่สัดส่วน F:C:W ที่ 5:10:10 ให้ค่ากำลังกด
สูงสุด ค่าสัมประสิทธิ์ความยืดหยุ่น ค่าแรงดึงสูงสุด ค่าแรงยึดหน่วงสูงสุด และค่าแรงเฉือนสูงสุด
เท่ากับ 10.45, 1360, 1.91, 2.23, และ 3.05 เมกะปาสคาลตามลำดับ ซึ่งมีค่ากำลังสูงกว่าสัดส่วน
B:C:W ค่าความซึมผ่านของทุกส่วนผสมจะลดลงในเชิงเวลาซึ่งมีค่าอยู่ในช่วง 10^{-9} ถึง 10^{-7} เมตรต่อ
วินาที และที่สัดส่วนของ F:C:W ที่ 5:10:10 จะให้ค่าความซึมผ่านต่ำที่สุด ในส่วนผสมรอยแตกที่มี
ระยะการเปิดแยกเท่ากับ 2, 10, และ 20 มิลลิเมตร จะให้ค่าความซึมผ่านใกล้เคียงกันอยู่ในช่วง 10^{-8}
ถึง 10^{-6} เมตรต่อวินาที

สาขาวิชา เทคโนโลยีธรณี
ปีการศึกษา 2559

ลายมือชื่อนักศึกษา อภิเชษฐ์ ใจดี
ลายมือชื่ออาจารย์ที่ปรึกษา P. Tepranun

MONTON CHIANGMAI : EXPERIMENTAL ASSESSMENT OF
MECHANICAL AND HYDRAULIC PERFORMANCE OF FLY ASH-MIXED-
CEMENT GROUTS IN ROCK FRACTURES. THESIS ADVISOR :
PRACHYA TEPNARONG, Ph.D., 107 PP.

FLY ASH/ GROUTING/ ROCK FRACTURE/ PERMEABILITY

The objective of this study is to assess the performance of fly ash mixed with the commercial grade Portland cement type I for use in reducing permeability of fractured rock in sandstone. The fractures are artificially made in Phu Kradung sandstone by applying a line load. The fly ash used in this study was obtained from the Mae Moh power plant. The physical and chemical properties of the fly ash are examined. This research emphasizes on determining the mixture that provides minimum slurry viscosity and appropriate strength. The mixing ratios for fly ash:cement:water (F:C:W) are 1:10:10, 3:10:10, 5:10:10 and bentonite:cement:water (B:C:W) are 1:10:10, 2:10:10, 3:10:10 by weight. These proportions yield the lowest slurry viscosity of 5 Pa·s. For F:C:W = 5:10:10, the compressive strength, elastic modulus, tensile strength, bond strength, and shear strength are 10.45, 1360, 1.91, 2.23, and 3.05 MPa, respectively. They are slightly higher than from those of bentonite mixed with cement. The permeability of grouting materials is from 10^{-9} to 10^{-7} m/s and decrease with curing time, the F:C:W = 5:10:10 gives the lowest permeability. The permeability of grouting fractures with apertures of 2, 10 and 20 mm range from 10^{-8} to 10^{-5} m/s.

School of Geotechnology

Academic Year 2016

Student's Signature 

Advisor's Signature 

ACKNOWLEDGMENTS

I wish to acknowledge the funding support of Suranaree University of Technology (SUT). I would like to express my sincere thanks to Dr. Prachya Tepnarong, thesis advisor, who gave a critical review and constant encouragement throughout the course of this research. Further appreciation is extended to Assoc. Prof. Dr. Pornkasem Jongpradist and Prof. Dr. Kittitep Fuenkajorn, for their constructive advice, valuable suggestions and comments on my research works as thesis committee members. Grateful thanks are given to all staffs of Geomechanics Research Unit, Institute of Engineering who supported my work.

Finally, I most gratefully acknowledge my parents and friends for all their supported throughout the period of this research.

Monton Chiangmai

มหาวิทยาลัยเทคโนโลยีสุรนารี

TABLE OF CONTENTS

	Page
ABSTRACT (THAI).....	I
ABSTRACT (ENGLISH).....	II
ACKNOWLEDGEMENTS.....	III
TABLE OF CONTENTS.....	IV
LIST OF TABLES.....	VIII
LIST OF FIGURES.....	X
SYMBOLS AND ABBREVIATIONS.....	XIV
CHAPTER	
I INTRODUCTION.....	1
1.1 Background of problems and significance of the study.....	1
1.2 Research objectives.....	2
1.3 Research methodology.....	2
1.3.1 Literature review.....	2
1.3.2 Sample collection and preparation.....	2
1.3.3 Permeability testing of fractures.....	3
1.3.4 Basic and hydraulic properties testing of grouting materials.....	3

TABLE OF CONTENTS (Continued)

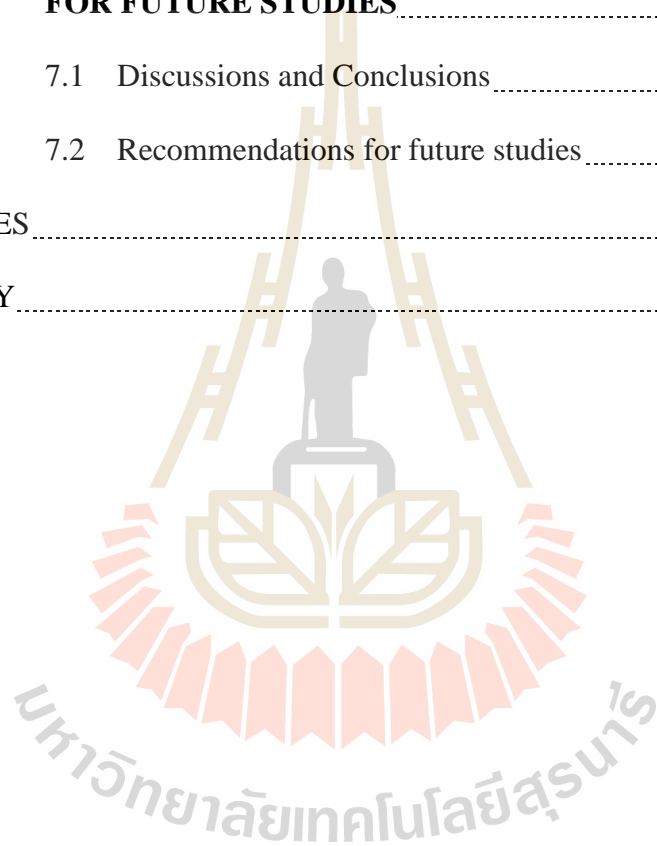
	Page
1.3.5 Mechanical Characterization testing of grouting materials.....	3
1.3.6 Data analysis and comparisons.....	4
1.3.7 Discussions and conclusions.....	5
1.3.8 Thesis writing.....	5
1.4 Scope and limitations of the study.....	7
1.5 Thesis contents.....	7
II LITERATURE REVIEW	9
2.1 Introduction.....	9
2.2 Experimental researches on the fly ash.....	9
2.3 Permeability of Single Fracture.....	11
2.4 Experimental researches on grouting materials.....	15
III SAMPLE PREPARATION	24
3.1 Introduction.....	24
3.2 Fly ash preparation.....	24
3.3 Bentonite.....	28
3.4 Portland cement.....	29
3.5 Rock samples.....	31
3.5.1 Sample preparation for constant head flow test under various normal stresses.....	32

TABLE OF CONTENTS (Continued)

	Page
3.5.2 Sample preparation for direct shear test under various normal stresses.....	33
IV GROUT PREPARATIONS	34
4.1 Introduction.....	34
4.2 Viscosity and density of mixtures.....	34
4.2.1 Test methods.....	38
4.2.2 Test results.....	43
V MECHANICAL PROPERTIES TESTING	46
5.1 Introduction.....	46
5.2 Basic Mechanical Properties Tests of Cement Grout.....	46
5.2.1 Uniaxial compressive strength testing.....	46
5.2.2 Brazilian tensile strength tests.....	58
5.2.3 Push-out test.....	60
5.2.4 Shearing resistance between grout and fracture.....	61
VI HYDRAULIC PROPERTIES TESTING	70
6.1 Introduction.....	70
6.2 Permeability of grouting materials.....	70
6.3 Permeability of rock fractures.....	74
6.4 Permeability of grouting materials in rock fractures.....	79

TABLE OF CONTENTS (Continued)

	Page
VII DISCUSSIONS, CONCLUSIONS AND RECOMMENDATIONS	
FOR FUTURE STUDIES	91
7.1 Discussions and Conclusions.....	91
7.2 Recommendations for future studies.....	94
REFERENCES.....	95
BIOGRAPHY.....	107



LIST OF TABLES

Table	Page
2.1 Normal range of chemical compositions for fly ash produced from different coal types	10
3.1 Atterberg's limits and specific gravity of fly ash, sludge and bentonite	27
3.2 Results of oxide concentrations in the bentonite and fly ash samples.....	29
3.3 Results of oxide concentrations in Portland cement.....	30
4.1 Results of slurry density tests in beakers of 500 cc.....	42
4.2 Results of slurry viscosity tests in beakers of 500 cc.....	45
5.1 Summary of parameters and results for basic mechanical of Uniaxial compressive testing at curing time 3 days.....	48
5.2 Summary of parameters and results for basic mechanical of Brazilian tensile testing at curing time 3 days.....	50
5.3 Summary of parameters and results for basic mechanical of push out testing at curing time 3 days	52
5.4 Summary of parameters and results for basic mechanical of Direct shear testing at curing time 3 days	53
5.5 Summary of Uniaxial strength, elastic modulus and poisson's ratio results on the F:C:W, and B:C:W mixtures specimens of 54.00 mm diameter	56
5.6 Summary of Brazilian tensile strength test results on the F:C:W, and B:C:W mixtures specimens	59

LIST OF TABLES (Continued)

Table	Page
5.7 Summary of push-out test average shear strength test results on the F:C:W mixtures specimens.	64
5.8 Summary of Direct shear strength test results on the F:C:W, and B:CW, mixtures specimens.	66
5.9 Summary of shear strength parameters calibrated from direct shear tests using Coulomb's criteria.	69
6.1 Summary of permeability testing of grouting material results at 3, 7, 14, 28, and 60 days of curing time.	73
6.2 Summary of permeability of rock fractures results.	77
6.3 Summary of permeability of grouting material in rock fractures aperture 2 mm.	82
6.4 Summary of permeability of grouting material in rock fractures aperture 10 mm.	84
6.5 Summary of permeability of grouting material in rock fractures aperture 20 mm.	86

LIST OF FIGURES

Figure	Page
1.1	Research methodology6
3.1	Fly ash from The Electricity Generating Authority of Thailand, Mae Moh power plant.....25
3.2	Fly ash samples are packed in a moisture barrier bucket. 25
3.3	Grain size distribution of fly ash compared water treatment sludge results26
3.4	Some sandstone samples with 130×130×130 mm ³ prismatic blocks for series for constant head flow testing31
3.5	Some sandstone samples with a width dimension of 54 mm and 108 mm of length for direct shear testing32
4.1	Fly ash from The Electricity Generating Authority of Thailand, Mae Moh used in this study35
4.2	Thai Nippon chemical industry Bentonite used in this study.....35
4.3	Bag of Portland cement 50 kg is used in this study.....36
4.4	Digital weight scale with maximum capacity for 2000 grams and accuracy to ± 0.01 gram.....36
4.5	Mixer, Kitchen aid Professional 600 6QT 575 watt stand mixer, with maximum capacity for 5,000 cm ³ and 6 speed control37
4.6	Viscometer, Book field viscometer RV 203 Watt 50 Hz37

LIST OF FIGURES (Continued)

Figure	Page
4.7	Laser thermometers TAITAN T350C with range -50 ~ 350° C38
4.8	Grouting materials in beakers are prepared for mix proportion (a) cement and water, (b) cement, water and fly ash, and (c) bentonite, cement and water.....39
4.9	Slurry volume of 500 cc in beakers for the density and viscosity tests (a) cement paste (b) sludge-cement slurry, and (c) bentonite-cement slurry41
4.10	Brookfield model RV dial reading viscometer is used for viscosity and slurry density tests44
4.11	Kinematic viscosity of bentonite-cement, sludge-cement and fly ash-cement mixtures for different W:C ratios44
5.1	Core sample is cut to obtain the desired length with Husqvarna Construction Products 433-81 Gothenburg Sweden47
5.2	Uniaxial compressive strength test with constant loading rate. The cylindrical specimen is loaded vertically using the compression machine.54
5.3	Some specimens prepared for basic mechanical testing (a) before testing, and (b) after testing55
5.4	Uniaxial compressive strengths fly ash-mixed cement as a function of curing time.....57
5.5	Elastic modulus fly ash-mixed cement as a function of curing time.....57
5.6	Brazilian tensile strength test with constant loading rate58
5.7	Some specimens prepared for Brazilian tensile strength testing59

LIST OF FIGURES (Continued)

Figure	Page
5.8	Brazilian tensile strength fly ash-mixed cement as a function of curing time..... 60
5.9	Bond strength testing (a) the schematic drawing of the push-out test, and (b) push-out test setup62
5.10	(a) Some sandstone specimen for push-out test, and (b) a cut section of specimen after failure in the push-out test63
5.11	Bond strength test fly ash-mixed cement as a function of curing time64
5.12	The direct shear machine model EL-77-1030 for direct shear tests65
5.13	Some specimens of 54×54×108 mm prepared for direct shear testing66
5.14	Shear stress as a function of shear displacement for pure cement67
5.15	Shear stress as a function of shear displacement for F:C:W=1:10:10.....67
5.16	Shear stress as a function of shear displacement for F:C:W=3:10:1068
5.17	Shear stress as a function of shear displacement for F:C:W=5:10:10.....68
5.18	Shear stress as a function of normal stress69
6.1	PVC mold has an inner diameter of 101.6 mm for permeability testing of grouting materials.....71
6.2	PVC mold has sealed between two acrylic platens with the aid of O-ring rubber and epoxy coating for permeability testing of grouting materials.....72
6.3	Diagram of laboratory arrangement for permeability testing of grouting materials72

LIST OF FIGURES (Continued)

Figure	Page
6.4	Laboratory arrangement for permeability testing of grouting materials73
6.5	Intrinsic permeability as a function of time for B:C:W, and F:C:W.....74
6.6	Some sandstone specimens of $130 \times 130 \times 130 \text{ mm}^3$ prepared for permeability testing of rock fractures75
6.7	Fracture surface in sandstone specimen prepared for permeability testing of rock fractures76
6.8	Laboratory arrangement for permeability testing of fractures76
6.9	Intrinsic permeability (k), hydraulic conductivity (K), and aperture (e_n) as a function of normal stress (σ_n) for fracture in Phu Kradung sandstone.....78
6.10	Some sandstone specimens prepared for permeability testing of grouting materials in rock fractures at fracture aperture 2, 10, and 20 mm.....79
6.11	Diagram of laboratory arrangement for permeability testing of grouting materials in rock fracture.....80
6.12	Permeability testing of grouting materials in rock fracture.....80
6.13	Intrinsic permeability (k), hydraulic conductivity (K), and aperture (e_h) as a function of normal stress (σ_n) for fracture aperture 2 mm.....88
6.14	Intrinsic permeability (k), hydraulic conductivity (K), and aperture (e_n) as a function of normal stress (σ_n) for fracture aperture 10 mm89
6.15	Intrinsic permeability (k), hydraulic conductivity (K), and aperture (e_n) as a function of normal stress (σ_n) for fracture aperture 20 mm90

SYMBOLS AND ABBREVIATIONS

ROMAN ABBREVIATIONS:

A	=	Cross-section area
A, B, m	=	Constants
b	=	Spacing between fracture
B:C:W	=	Proportion of bentonite-mixed cement or bentonite:cement:water
C	=	Portland cement
C_0	=	Constant depends on fracture surface and initial joint aperture
c_p	=	Cohesion
D	=	Diameter of the injection hole at the center of the upper block
E	=	Elastic modulus
e	=	Hydraulic aperture
e_0	=	Hydraulic aperture at zero stress
e_0	=	Initial joint aperture
e_h	=	Hydraulic aperture
F	=	Sheared force
F:C:W	=	Proportion of fly ash-mixed cement or fly ash:cement:water
g	=	Acceleration due to gravity
Hc	=	Constant head
K	=	Hydraulic conductivity between smooth and parallel plates
k	=	Intrinsic permeability

SYMBOLS AND ABBREVIATIONS (Continued)

k_0	=	Initial fracture permeability at initial normal stress
K_f	=	Fracture conductivity
K_n	=	Normal stiffness of discontinuity
L	=	Thickness of grouting material in fracture apertures
L/D	=	Length to diameter ratio
M	=	Constant is equal to 1
P	=	Normal load
P_1	=	Effective modulus of the asperities
P_f	=	Maximum load
p_w	=	Water pressure within the discontinuity
Q	=	Flow rate
q	=	Water flow rate through the specimen
r	=	Radius of flow path
r_0	=	Radius of the radius injection hole
s	=	Fracture spacing
$S:C:W$	=	Proportion of sludge-mixed cement or sludge:cement:water
SG	=	Specific gravity
t	=	Thickness of sample
T_{Slurry}	=	Temperature of slurry
$W:C$	=	Water-cement ratio or water:cement
W_{Slurry}	=	Weight of slurry

SYMBOLS AND ABBREVIATIONS (Continued)

GREEK ABBREVIATIONS:

β	=	Orientation of discontinuity
μ	=	Dynamic viscosity
τ	=	Shear stress
ρ	=	Slurry density
v_1	=	Normal deformation of the joint
ν	=	Kinetic viscosity
v_0	=	Closure of the joint when the hydraulic aperture becomes zero
σ, σ_n	=	Normal stress
σ_0	=	Initial normal stress
σ_B	=	Brazilian tensile stress
σ_c	=	Compressive strength or effective confining stress
σ_{ch}	=	Confining healing pressure in which the permeability is zero
σ_h	=	Horizontal stress applied to the discontinuity
σ_z	=	Vertical stress applied to the discontinuity
δe	=	Change of the joint aperture due to stresses
δe_n	=	Normal deformation component
ΔP	=	Injecting water pressure
ρ_{slurry}	=	density of mixture slurry
ρ_w	=	Density of distilled water at the time of measurement

SYMBOLS AND ABBREVIATIONS (Continued)

- γ_w = Unit weight of water
- μ = Dynamic viscosity of the water
- ϕ_p = Angle of internal friction



CHAPTER I

INTRODUCTION

1.1 Background of problems and significance of the study

The increasing amount of the fly ash from burning process of lignite coal for uses to generate the electricity at Mae Moh mine has collected for permanent solutions to dispose of the fly ash at the Electricity Generating Authority of the Mae Moh power plant. A report indicates that the plant produces fly ash with the maximum capacity of 6,000 tons/day. Since 1997, many researchers have been studied and attempted to utilize the disposed fly ash for reduction of the landfill problem. These solutions are mixing the fly ash with the cement for use in the dam, foundation, and construction materials (cement roofs, tiles, and waste water pipes). One of the solutions is to apply the fly ash to minimizing groundwater flow in rock fractures. Groundwater in the rock mass is one of the key factors governing the mechanical stability of slope embankments, underground mines, tunnels, and dam foundation. A common solution practiced internationally in the construction industry is to use bentonite mixed with cement as a grouting material to reduce permeability in the fractured rock mass. Knowledge and experimental evidence about the permeability of the fly ash mixed cement in fractured rock have never been addressed. The objective of this study is to assess the performance of fly ash mixed with the commercial grade Portland cement for reducing permeability in saturated fractured

rock in the laboratory and to compare the results with those of bentonite mixed cement in terms of the mechanical and hydraulic performance.

1.2 Research objectives

The objectives of this study are to experimentally assess the performance of fly ash mixed with Portland cement for grouting in fractured rock under various stresses in the laboratory and to compare the results with the bentonite-mixed cement in terms of the mechanical and hydraulic properties. The cement grout is prepared by the commercial grade Portland cement mixed with fly ash from Mae Moh power plant. The results are used in the design of cement grout in fractured rock to minimize the permeability in the rock mass.

1.3 Research methodology

1.3.1 Literature review

This chapter summarizes the results of literature review carried out to improve an understanding of the fly ash, grouting material, and permeability of single fracture. The sources of information are from textbooks, journals, and conference papers.

1.3.2 Sample collection and preparation

The grouting materials and rock samples used in this research are 1) the fly ash with particle sizes less than 75 μm , 2) commercial grade bentonite for comparing with the fly ash test results, 3) commercial grade Portland cement type I for mixing with the fly ash and bentonite, and 4) rock fracture samples from sandstone, limestone and granite. Sample preparation is carried out in the

Geomechanics Research (GMR) Laboratory at Suranaree University of Technology. The fly ash is collected from the Mae Moh power plant Electricity Generating Authority of Thailand.

1.3.3 Permeability testing of fractures

Before grouting with fly ash-mixed cement or bentonite-mixed cement into the artificial fracture of the sandstone specimens, the fracture permeability needed to be measured. The fracture permeability is used to compare with the permeability of grouting materials for both fly ash and bentonite. The constant head flow tests are performed to determine the fracture permeability of sandstone specimens under normal stresses. The normal stresses are ranging from 0.25 to 1.25 MPa. The results simulate stress under various depths which can affect the permeability of grouting materials in fractured rock.

1.3.4 Basic and hydraulic properties testing of grouting materials

The objective of these tests is to determine density, grain size, atterberg's limits viscosity, and permeability of fly ash and bentonite-mixed cement. The fly ash and bentonite-mixed cement ratios vary from 1:10, 2:10, 3:10, 4:10, and 5:10 for selecting the optimum mixing content. Similarities and differences of the results are compared.

1.3.5 Mechanical Characterization testing of grouting materials.

1.3.5.1 Uniaxial compressive strength testing of grouting materials

The objective of the uniaxial compressive strength tests is to determine the uniaxial compressive strength and elastic modulus of grouting material specimens. Grouting materials are fly ash-mixed cement and bentonite-mixed cement. The test procedure is similar to the ASTM standards (ASTM C938, D4832

and C39). The fly ash and bentonite-mixed cement ratios vary from 1:10, 2:10, 3:10, 4:10, and 5:10 for determining the strength and the elastic modulus.

1.3.5.2 Brazilian tensile strength testing of grouting materials

The Brazilian tension test determined the indirect tensile strength of the cement grouts. The test procedure follows the ASTM (D3967) and the ISRM suggested method. One hundreds samples with a diameter of 54 mm are tested with $L/D = 0.5$.

1.3.5.3 Direct sheared testing of grouting materials

The objective of the direct sheared tests is to determine the shear strength of grouting material in sandstone fracture. Grouting materials are fly ash and bentonite-mixed cement. The experimental procedure is similar to the ASTM standard (D5607). The constant normal stresses are 0.25, 0.5, 1.0 and 1.25 MPa. The shear stress is applied while the shear displacement and head drop is monitored for every 0.2 mm of shear displacement. Similarities and differences of the results are compared with other researches.

1.3.5.4 Push-out test

Push out test determined the push out strength of cement grout casted in a hole at the center of the specimen with a diameter of 45 mm and length of 130 mm. The cement grouts casted in the hole at the center of Phu Kradung sandstone are investigated after 28 days curing.

1.3.6 Data analysis and comparisons

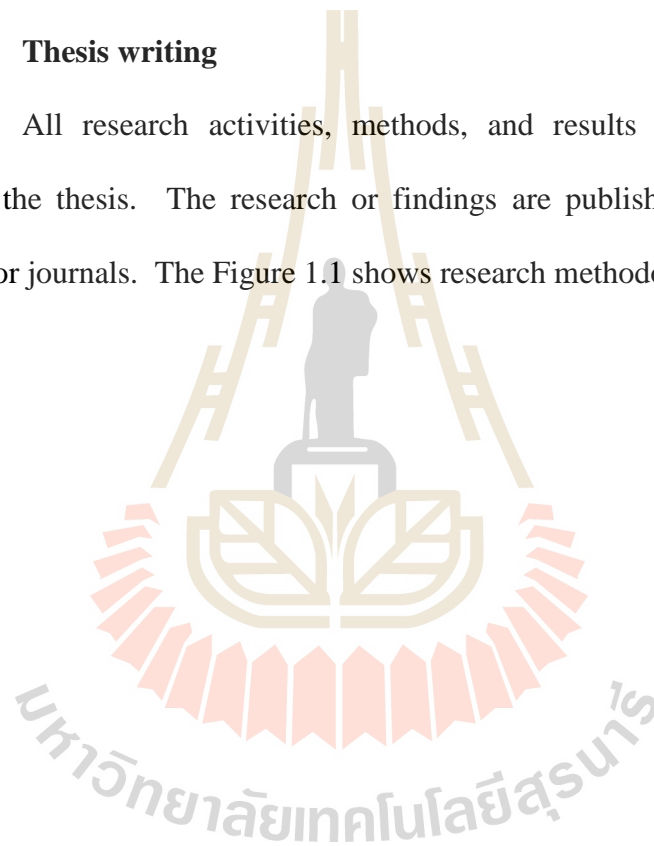
The research results are analyzed to optimize the grout mix ratios in terms of the mechanical and hydraulic properties. The results of the analysis are used in the comparison with other researchers.

1.3.7 Discussions and conclusions

Discussions of the results are described to determine the reliability and accuracy of the measurements. Performance of the new grouting material is discussed based on the test results. Similarities and discrepancies of the grouting materials in terms of the mechanical and hydraulic properties are discussed to apply the fly ash mixed cement in the fields.

1.3.8 Thesis writing

All research activities, methods, and results are documented and compiled in the thesis. The research or findings are published in the conference proceedings or journals. The Figure 1.1 shows research methodology for this study.



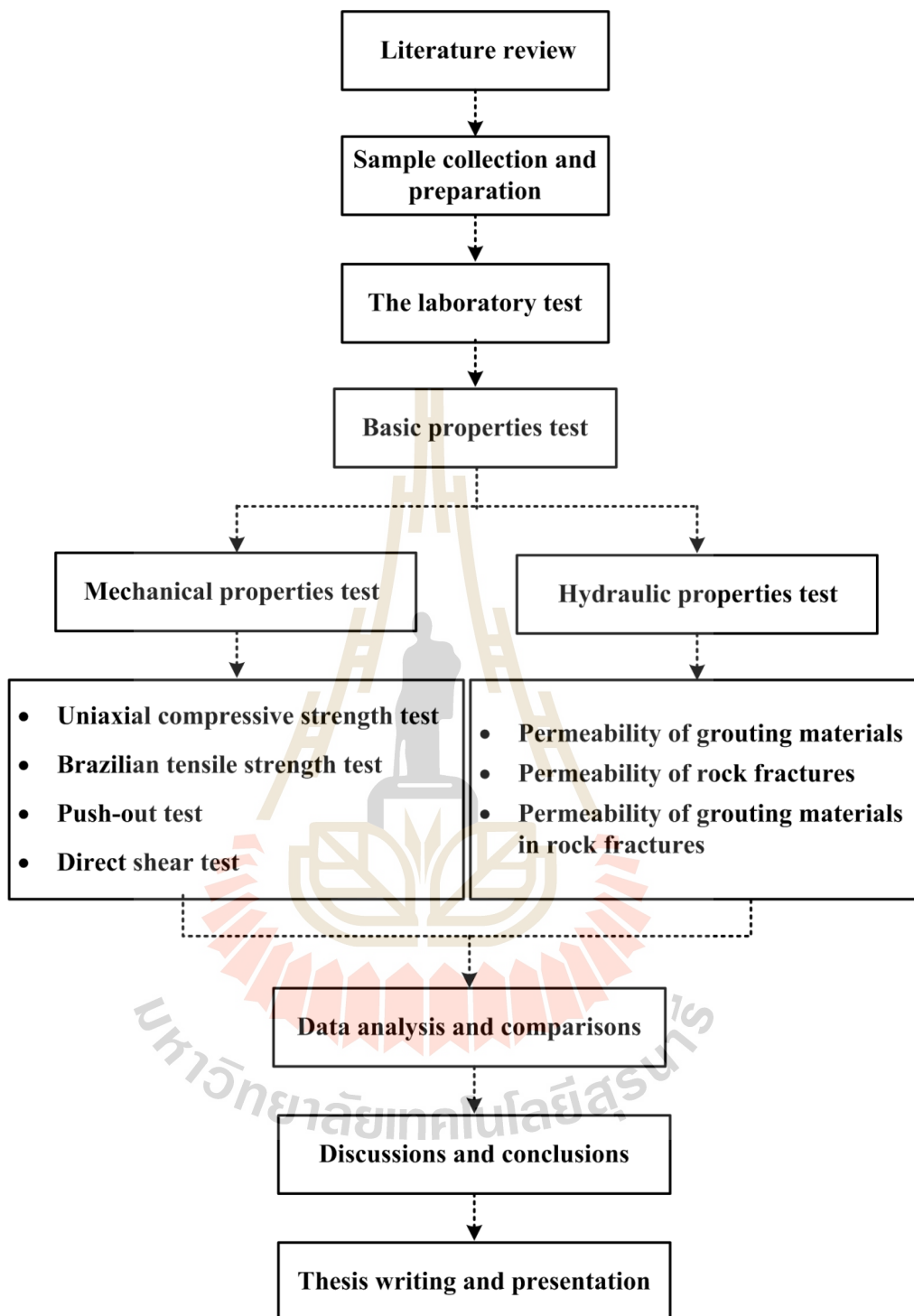


Figure 1.1 Research methodology.

1.4 Scope and limitations of the study

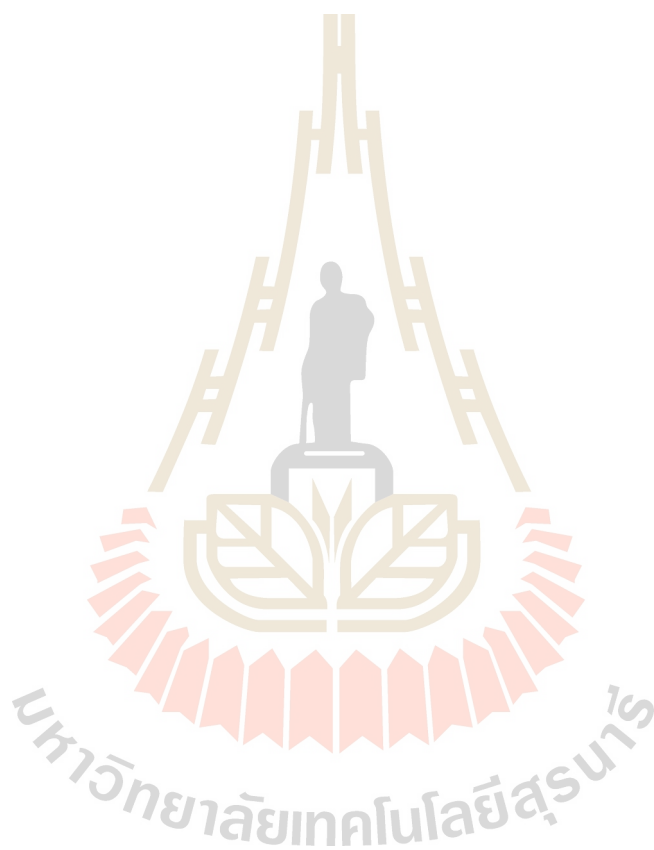
The scope and limitation of the research include as follows.

1. This research emphasizes on studying the mechanical and hydraulic properties of fly ash-mixed cement as a grouting material to reduce permeability in fractured rock mass.
2. The laboratory tests of permeability fly ash mixed cement include constant head flow tests and uniaxial compression test.
3. Portland cement type I as follows (ASTM C150).
4. The particle sizes of the fly ash are less than 0.075 mm (sieve no. 200).
5. The fly ash-to-cement (by dry weight) ratios of 1:10, 3:10 and 5:10 are primarily selected.
6. Laboratory testing is conducted on specimens from sandstone. The cross-section area fracture is $130 \times 130 \text{ mm}^2$.
7. All tested fractures are artificially made in the laboratory.
8. Mixing, curing and testing of the cement and mixtures follows, as much as practical, the ASTM standards.
9. Compare the result with those of the fly ash and bentonite mixed cement in them engineering properties.

1.5 Thesis contents

Chapter I introduces the thesis by briefly describing the background of problems and significance of the study. The research objectives, methodology, scope and limitations are identified. **Chapter II** summarizes the results of the literature review. **Chapter III** describes the sample and mixture preparations. **Chapter IV** to

VI describes the results from the laboratory experiments. The experiments are divided into 3 tests, including 1) Basic properties testing 2) Mechanical properties test 3) Hydraulic properties test. **Chapter VII** and **VIII** discussions and conclusions the research results, and provides recommendations for future research studies.



CHAPTER II

LITERATURE REVIEW

2.1 Introduction

This chapter summarizes the results of literature review carried out to improve an understanding of the fly ash, grouting material, and permeability of single fracture. The sources of information are from textbooks, journals, and conference papers.

2.2 Experimental researches on the fly ash

Fly ash (or Pulverized Fuel Ash) from the coal burning, and is trapped by static dust catcher system. The ash has a fine brownish-gray powder. The fly ash quality depends on the quality of coal (anthracite, bituminous, sub-bituminous, lignite). In Thailand, the lignite coal is classified to a low-grade quality, and hence obtained the low quality of fly ash. Mae Moh power plant, Lampang province is the main source of fly ash in Thailand. They use the lignite coal (some sub-bituminous) as fuel for boiling to generate electricity. The process produced the fly ash about 3×10^6 tons/year which is relatively low quality. There are however enormous quantities, and hence it requires a large area for landfilling.

Zimmer (1970) suggested that fly ash can be classified into two types that depend on the chemical compositions and source of fly ash. The two classes of fly ash are defined according to ASTM C618 (ISG resources, Headwater Company):

Class F fly ash and Class C fly ash. The main difference between these classes is the differing amount of calcium, silica, alumina, and iron content in the ash. The chemical properties of fly ash are largely determined by the chemical content of the coal burned. Table 1 shows typical examples of ash compositions resulting from the burning of various types of coals.

Table 2.1 Normal range of chemical compositions for fly ash produced from different coal types (Zimmer, 1970).

Components	Anthracite	Bituminous	Subbituminous	Lignite
SiO ₂ (%)	80-90	20-60	40-60	15-45
Al ₂ O ₃ (%)	0-5	5-35	20-30	20-25
Fe ₂ O ₃ (%)	0-3	10-40	4-10	4-15
CaO (%)	0-1	1-10	5-30	15-40
SO ₃ (%)	0-1	0-5	2-7	5-10
LOI* (%)	0-2	0-15	0-3	0-5

*LOI = Loss of ignition

Cheerarat and Jaturapitakkul (2004) found that the generation of electricity and process heat from coal combustion without proper and efficient handling of emitted ash particles cause severe impact on the environment. In the past, fly ash was generally released into the atmosphere, but pollution control equipment mandated in recent decades now requires that it be captured prior to release. Electrostatic precipitators are typically used to control the entrained particulates while the reduction of SO₂ emission is achieved with flue gas desulfurization equipment (scrubbers). Worldwide, more than 65% of the captured fly ash from coal-fired power stations is disposed of in landfill and ash ponds. In Thailand, almost all power

plants are a thermal power plant that burns lignite coal to produce electrical energy. During the early of 1970–2000, approximately 50×10^6 tons of fly ash and bottom ash were disposed of by the open landfill method.

Nimjaroen (2013) suggested that fly ash consists of inorganic, incombustible matter presenting in the coal that has been fused during combustion into a glassy, amorphous structure. It consists mostly of silica (SiO_2), alumina (Al_2O_3), iron oxides ($\text{FeO} + \text{Fe}_2\text{O}_3$), alkali and alkaline earth oxides with a small amount of various heavy metals and transition metal oxides (Barbieri et al., 2000). Coal burning generates heat and residue that contains 80 percent fly ash and 20 percent bottom ash which can be classified by the location and methods of recovery. Fly ash particles are generally spherical in shape and range in size from $0.5 \mu\text{m}$ to $100 \mu\text{m}$. They are also pozzolanic in nature and can react with calcium hydroxide and alkali to form calcium silicate hydrates (cementations compounds).

2.3 Permeability of Single Fracture

The main factors controlling fluid flow through a single fracture are the surface roughness, apertures, orientation of fractures, normal and shear stresses, and unloading behavior. Out of these controlling factors, the aperture is the major parameter, which is a function of external stress, fluid pressure and geometrical properties of the fracture (Indraratna and Ranjith, 2001).

The conductivity of a single fracture is given by the ‘cubic law’: (Witherspoon et al., 1980; Indraratna and Ranjith, 2001; Ranjith and Viete, 2011)

$$K_f = ge^3/12vb \quad (2.1)$$

where K_f = fracture conductivity (m/s), e = hydraulic aperture (m), g = acceleration due to gravity (m/s^2), ν = kinematic viscosity, which is 1.01×10^{-6} (m^2/s) for pure water at $20^\circ C$, and b is the spacing between fracture (m).

For a smooth, planar joint having an aperture of magnitude e , the fracture permeability (k) for laminar flow is given by (Barton et al., 1985)

$$k = e^2/12 \quad (2.2)$$

The joint aperture e is mainly dependent on the normal and shear stress acting on the joint. Assuming the rock matrix to be isotropic and linear elastic, obeying Hooke's law, the following aperture-stress relationship can be formulated: (Rutqvist, 1995; Indraratna and Ranjith, 2001)

$$e = e_0 \pm \delta e \quad (2.3)$$

where e_0 is the initial joint aperture and δe is the change of the joint aperture due to stresses (i.e., both normal and shear components) acting on the joint. In conventional rock mechanics, the normal deformation component is given by Jaeger and Cook (1979):

$$\delta e_n = (1/K_n)(\sigma_z \cos \beta + \sigma_h \sin \beta) \quad (2.4)$$

where K_n = normal stiffness of discontinuity, σ_z = vertical stress applied to the discontinuity, σ_h = horizontal stress applied to the discontinuity, and β = orientation of discontinuity.

Considering the water pressure to be acting perpendicular to the joint surface, the equation can be modified to obtain (Indraratna and Ranjith, 2001)

$$\delta e_n = (1/K_n)(\sigma_1 \cos \beta - \sigma_3 \sin \beta - p_w) \quad (2.5)$$

where p_w = water pressure within the discontinuity.

Combining the above equations for planar and smooth joints, the permeability of a single fracture is given by

$$k = (e_0 + \delta e_n)^2 / 12 \quad (2.6)$$

Based on the initial hydraulic aperture and the closure of joint, Detoumay (1980) suggested the following relationship to determine the fracture permeability:

$$k = e_0^2 (1 - v/v_0)^2 / 12 \quad (2.7)$$

where e_0 = hydraulic aperture at zero stress, v_0 = closure of the joint when the hydraulic aperture becomes zero and v = normal deformation of the joint.

Snow (1968) observed an empirical model to describe the fracture fluid flow variation against the normal stress, as described by

$$k = k_0 + K_n (e^2/s) (\sigma - \sigma_0) \quad (2.8)$$

where k_0 = initial fracture permeability at initial normal stress (σ_0), K_n = normal stiffness, s = fracture spacing and e = hydraulic aperture.

Jones (1975) suggested the following empirical relation between the fracture permeability and the normal stress:

$$k = C_0[\log(\sigma_{ch}/\sigma_c)]^3 \quad (2.9)$$

where σ_{ch} = confining healing pressure in which the permeability is zero and σ_c = effective confining stress. The constant (C_0) depends on the fracture surface and the initial joint aperture.

Nelson (1975) suggested the following empirical relation between the fracture permeability and the normal stress:

$$k = A + B\sigma_c^{-m} \quad (2.10)$$

where A , B and m are constants which are determined by regression analysis. These constants may vary from one rock to another, and even for the same rock type, depending on the topography of the fracture surface.

Gangi (1978) reported a theoretical model for fracture permeability as a function of the confining pressure, as represented by:

$$k = k_0[1 - (\sigma_c/P_1)^m]^3 \quad (2.11)$$

where P_1 = effective modulus of the asperities and m = constant which describes the distribution function of the asperity length. This expression gives a better prediction if the effect of surface roughness on flow is negligible, which of course is not reasonable in practice.

2.4 Experimental researches on grouting materials

Huang (1997) investigated the properties of cement-fly ash grout mixtures as barriers for isolation of hazardous and low-level radioactive wastes. The fly ash was used to replace 30 percent by mass of cement. Three additives, including bentonite, silica fume, and polypropylene fiber were used individually in the grout mixes to improve the properties of the grouts in different aspects. The flow ability, bleeding, and setting time of freshly mixed grouts were determined; and the unconfined compressive strength, pore size distribution, and water permeability were determined for hardened grouts at various curing durations up to 120 days. Finally, the durability of cement-fly ash grouts was carefully examined in terms of the changes in their physical properties after different levels of exposure to sulfate attack and wet-dry cycles.

Owaidat et al. (1999) reported that the U.S. Army Corps of Engineers had recently implemented a levee-strengthening program along the banks of the American River in Sacramento, California. During the rainy season, the existing levee system protected major commercial and residential areas of this metropolitan area. One of the main components of this program was the construction of slurry walls through the existing levee to improve stability by preventing seepage through and beneath the levee. Since conventional soil-bentonite (SB) slurry walls had little shear strength, which would jeopardize the stability, of the existing levees, and cement-bentonite (CB) slurry walls were significantly more expensive, soil-cement-bentonite (SCB) slurry walls were being utilized for this strengthening program. This research described a case study on the design, construction and performance of an underground SCB barrier wall, which was used to isolate river water seeping into the American

River levee and its foundation soils. Challenges to barrier performance included achieving a maximum allowable hydraulic conductivity of 5×10^{-7} cm/s while having a minimum unconfined compressive strength of 15 psi.

Kashir and Yanful (2000) reported that the use of slurry walls to contain oxidized tailings and provide cutoff below tailings dams were generally a cost-effective way of preventing environmental degradation due to seepage of acid water from tailing's areas. Long-term environmental protection dictated that the slurry wall materials been compatible with the acid water. Six percent bentonite by weight was added separately to two natural soils to represent slurry wall backfill materials, which were then permeated with several pore volumes of acid mine drainage (AMD) in the laboratory. Results using both flexible wall and fixed wall permeameters were similar. The carbonate-rich backfill gave an average hydraulic conductivity (K) of 1×10^{-9} cm/s, buffered the AMD at circumneutral pH, and kept effluent metal concentrations to very low values, for example, less than 0.05 mg/l zinc. The carbonate-free backfill also maintained low K (average 3×10^{-9} cm/s) during AMD permeation, it could not neutralize the AMD as effluent pH decreased to approximately 3.5, and metal concentrations reached those of the influent or permeant after about 17 pore volumes.

Fransson (2001) described a rock volume suitable for a grouting field test at the Äspö Hard Rock Laboratory, Sweden. Fixed interval length transmissivities and the corresponding number of fractures from geological mapping of a probe hole were used to calculate a probability of conductive fractures for analyses of data from individual boreholes. The transmissivity and specific capacity of the boreholes were compared to examine the robustness of the specific capacity. From the findings of the

study, the probability of conductive fractures from probe hole data, the specific capacity and fracture frequency of individual boreholes were sufficient to construct a simplified model of the fracture and the rock volume. The median specific capacity of the boreholes was a good description of the effective cross-fracture transmissivity. The field test was also carried out to demonstrate the usefulness of the methodology for improving the analyses of data from the hydraulic tests and geological mapping for a grouting fan.

Ryan and Day (2002) stated that Soil-Cement-Bentonite (SCB) slurry walls had been used with increasing frequency in recent years to provide barriers to the lateral flow of groundwater in situations where the strength of a normal soil-bentonite (SB) wall would be inadequate to carry foundation loads. The addition of cement to the backfill blended allows the backfill to set and form a more rigid system that could support greater overlying loads. Construction and quality control for the SCB wall were more demanding than that needed for the SB walls. Backfill mixing, sampling and testing of this type of wall involve more exacting procedures. Recommendations were made for methods to carry out pre-job design mix testing and in-field quality control testing for the most reliable results. Designing the SCB backfill was a complex issue involving conflicting actions of the various materials involved. While the SCB wall provides additional strength, permeability was one property that generally suffers in comparison to the SB walls. A normal permeability specification would be a maximum of 1×10^{-6} cm/sec. With special attention to materials and procedures, a specification of a maximum 5×10^{-7} could be achieved. The results were presented that the strengths of the SCB were in the range of 15-300 psi.

Rahmani (2004) stated that grouting had been used over the past two centuries to increase the strength, decrease the deformation and reduce the permeability of soils or fractured rocks. Due to its significance in engineering and science predicting grout effectiveness in fractured rocks was of interest. There were different approaches to estimate the effectiveness of grouting, one of which was numerical modeling. Numerical models could simulate a distribution of grout inside fractures by which the effectiveness of grout could be estimated. Few numerical studies had been carried out to model grout penetration in fractured rocks. Due to complexities of modeling grout and fracture most of these studies had either used simplifying assumptions or been bound to small sizes of fractures, both resulting in unrealistic simulations.

Then the current work is aimed to eliminate some of the simplifying assumptions and to develop a model that could improve the reliability of the results. In reality, grouts were believed to behave as a Bingham fluid, but many models did not consider a full Bingham fluid flow solution due to its complexity. Real fractures had rough surfaces with randomly varying apertures. However, some models considered fractures as planes with two parallel sides and a constant aperture. In this work the Bingham fluid flow equations were solved numerically over a stochastically varying aperture fracture. To simplify the equations and decrease the computational time the current model substituted two-dimensional elements by one-dimensional pipes with equivalent properties. The model was capable of simulating the time penetration of grout in a mesh of fracture over a rather long period of time. The results of the model could be used to predict the grout penetration for different conditions of fractures or grout (Rahmani, 2004).

Baik et al. (2007) described that compacting bentonite had been considered as a candidate buffer material in the underground repository for the disposal of high-level radioactive waste. An erosion of bentonite particles caused by a groundwater flow at the interface of a compacting bentonite, and fractured granite was studied experimentally under various geochemical conditions. The experimental results showed that bentonite particles could be eroded from a compacted bentonite buffer by a flowing groundwater depending upon the contact time, the flow rate of the groundwater, and the geochemical parameters of the groundwater such as the pH and ionic strength. A gel formation of the bentonite was observed to be a dominant process in the erosion of bentonite particles, although an intrusion of bentonite into a rock fracture also contributed to the erosion. The concentration of the eroded bentonite particles eroded by a flowing groundwater was increased with an increasing flow rate of the groundwater. It was observed from the experiments that the erosion of the bentonite particles was considerably affected by the ionic strength of a groundwater, although the effect of the pH was not great within the studied pH range from 7 to 10. An erosion of the bentonite particles in a natural groundwater was also observed to be considerable, and the eroded bentonite particles were expected to be stable at the given groundwater condition. The erosion of the bentonite particles by a flowing groundwater did not significantly reduce the physical stability and thus the performance of a compacted bentonite buffer. However, it was expected that an erosion of the bentonite particles due to a groundwater flow will generate bentonite particles in a given groundwater condition, which could serve as a source of the colloids facilitating radionuclide migration through rock fractures.

Butron et al. (2010) presented a new pre-excavation grouting concept to prevent dripping and reduced the inflow into a railway tunnel. For this purpose, the tunnel's roof was dripped-sealed using colloidal silica and the walls and invert of the tunnel were grouted with cement. The grouting design process followed a structured approach with pre-investigations of core-drilled boreholes providing parameters for the layout. Water pressure tests and pressure volume time recordings were used for the evaluation. Results showed that the design was successful: the total transmissivity was reduced from $4.9 \times 10^{-8} \text{ m}^2/\text{s}$ to the measurement limit ($1.6 \times 10^{-8} \text{ m}^2/\text{s}$), and the dripping was reduced to eight spots from the roof. Improved rock characterization showed that the grout hole separation was within the transmissivity correlation length and that grouting efficiency depends to a large extent on the dimensionality of the flow system of the rock mass.

Tepnarong (2013) studied the frictional shear strengths between cement grout and rock salt fracture have been experimentally determined by series of borehole push-out testing and direct shear testing. The salt specimens were prepared from the Maha Sarakham formation in the northeast of Thailand. The components of cement slurry are 700 g of Portland-pozzolan cement (type IP), 385 g of NaCl Saturated Brine, 20 g of Sika Plastocrete (anti-form agent) and 3.5 g of Sika Interplant ZX (liquid additive). The curing period for all push-out tests and direct shear tests was 3 days. According to the Coulomb criterion, the friction angles at the cement-salt interface are 70° and 69° for fracture and saw cut surfaces, respectively. The cohesion for the cement-salt fracture was averaged as 0.42 MPa. The push-out test results show significantly higher values of the frictional resistance at the interface than does the direct shear testing. The axial shear strength of the borehole cement

seal is as high as 7.05 to 11.23 MPa. This is primarily due to the effect of the Poisson's ratio which increases the normal (radial) stress at the cement-salt interface while the axial load is applied. This implies that the direct shear test results may give an over conservative estimate of the shearing resistance between the salt and cement seal.

Wetchasat and Fuenkajorn (2013) assessed the performance of sludge mixed with the commercial grade Portland cement type I for use in reducing permeability of fractures in sandstone. The fractures are artificially made in Phu Kradung sandstone by applying a line load to induce a splitting tensile crack in $0.15 \times 0.15 \times 0.15 \text{ m}^3$ prismatic blocks. The Bang Khen water treatment sludge is used. More than 80% of the sludge is quartz with grain size less than $75 \text{ }\mu\text{m}$. This study aims at determining the minimum slurry viscosity and appropriate strength of the grouting materials. The results indicate that the suitable mixing ratios for sludge: cement (S: C) are 1:10, 3:10, 5:10 with water-cement ratio (W:C) of 1:1 by weight. These proportions yield the lowest slurry viscosity of $5 \text{ Pa}\cdot\text{s}$. For S: C = 3:10, the compressive strength and elastic modulus are 1.22 MPa and 224 MPa which are similar to those of bentonite mixed with cement. The shear strength of grouted fractures varies from 0.22 to 0.90 MPa under normal stresses ranging from 0.25 to 1.25 MPa. The intrinsic permeability of grouting materials is from 10^{-17} to 10^{-15} m^2 and decreases with curing time. The S:C ratio of 5:10 gives the lowest permeability. The intrinsic Permeability of grouted fractures with apertures of 2, 10 and 20 mm range from 10^{-16} to 10^{-14} m^2 .

Tepnarong and Deethouw (2014) experimentally assessed the performance of sludge-mixed cement grouts for sealing boreholes in rock salt. The cement grout is prepared from the commercial grade Portland cement mixed with Bang Khen water

treatment sludge, brine, and chloride resistant agent. The results are used in the design of borehole seal in rock salt to minimize the brine circulation and potential leakage for the industrial waste repository. The rock salt specimens are prepared from the 54 mm diameter cores drilled from the Middle member of the Maha Sarakham formation. The results indicate that the viscosity of grout slurry tends to increase as the sludge-mixed cement (S:C) ratio increases. The permeability of the sludge-mixed cement grouting materials measured from the longitudinal flow test with constant head decreases with curing time at 7, 14, 21 and 28 days. The results indicate that when the curing time increases the intrinsic permeability (k) of cement grout decreases. The mixture with the S:C of 5:10 by weight gives the lowest permeability. The S: C mixtures have the mechanical and hydraulic properties equivalent to those of the commercial grade Portland cement mixtures which indicate that the sludge can be used as a substituted material to mix with cement for rock salt fracture grouting purpose. The compressive strength after 28 day curing times is 9.58 ± 0.52 MPa. The highest compressive strength is from S: C = 5:10. The average tensile strength is 1.99 ± 0.14 MPa. The highest bond strength is 7.49 MPa. The curing increases. Similarities and discrepancies of the grouting performance in terms of mechanical and hydraulic properties are compared.

Pattani and Tepnarong (2015) studied the frictional shear strengths of cement sealing in rock salt by series of borehole push-out testing and direct shear testing. The results are used to assist in design of the cement seals in the rock salt to minimize brine circulation and potential leakage along a main access of salt mine. The salt specimens are prepared from 100 mm diameter cores drilled from Middle member of the Maha Sarakham formation. The cement seal is prepared from commercial grade

Portland-pozzolan cement, saturated brine, anti-form agent and liquid additive. The cement slurry is cast in the 25 mm diameter borehole with a length of 30 mm for the push-out testing and on the 100 mm diameter fracture saw cut surface for the direct shear testing. For all tests the cement is cured for 7 days prior to testing. The results indicate that dynamic viscosity of grout slurry is 4.53 Pa.s. The curing time increases the intrinsic permeability of cement grout decreases. The uniaxial compressive and Brazilian tensile strengths after 28 day curing times are 20.06 ± 3.82 MPa and 2.89 ± 0.19 MPa, respectively. The direct shear tests results indicate the frictional resistance at cement-salt interface with a friction angle of 44 degrees and cohesion of 2.12 MPa. The normal stiffness is 7.67 GPa/m. The shear stiffness is 6.60 GPa/m. The push-out test results show significantly the higher frictional resistance at the interface than does the direct shear testing. The axial shear strength of the borehole cement seal is 5.05 MPa. The findings are useful for determination of initial installation parameters of the cement seals in salt mine openings.

CHAPTER III

SAMPLE PREPARATIONS

3.1 Introduction

This chapter describes basic characteristics of materials tested in this study. Materials used in this experiment consist of fly ash, bentonite, Portland cement and sandstone samples.

3.2 Fly ash preparation

Fly ash samples used in this research have been donated by The Electricity Generating Authority of Thailand, Mae Moh power plant. Fly ash from burning process of lignite coal for uses to generate the electricity has collected for a permanent solution to dispose of the fly ash (Figures 3.1). Fly ash can be classified into two types of Bottom ash about 20% and fly ash about 80%. Fly ash products have good pozzolan or binding properties and are therefore an excellent choice for construction material to substitute Portland Cement Type I at a much cheaper cost. Fly ash is classified as Class C by ASTM C618 standard. It has a spherical shape with its specific gravity of 2.00-2.60, free lime value of less than 3 %, and sulfur dioxide less than 5 %. The fly ash samples are collected and packed in a moisture barrier bucket (Figures 3.2).

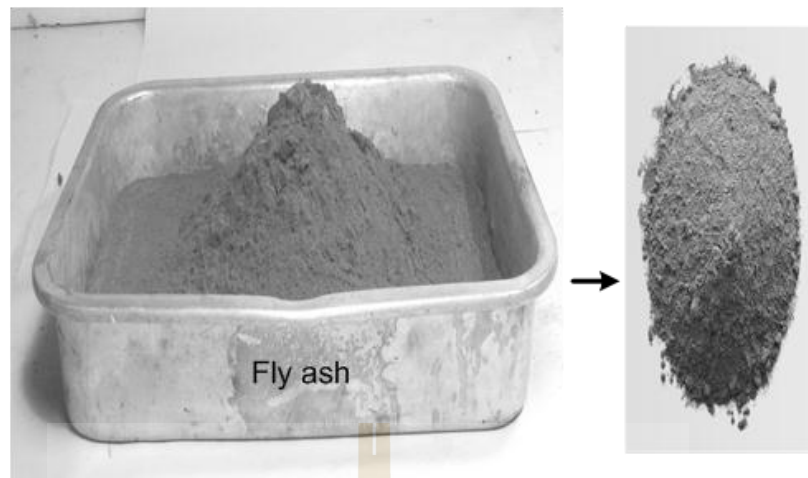


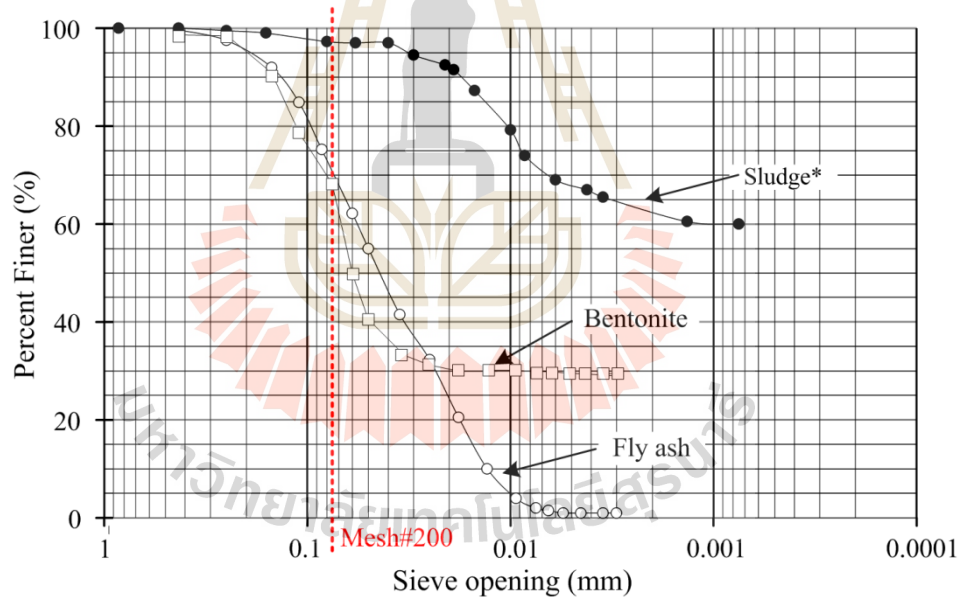
Figure 3.1 Fly ash from The Electricity Generating Authority of Thailand, Mae Moh power plant.



Figure 3.2 Fly ash samples are packed in a moisture barrier bucket.

One of the basic physical properties of the fly ash is the distribution of the grain size particles. The distribution of different grain sizes affects the engineering

properties of fly ash. Grain size analysis provides the grain size distribution of material ranging from 0.001-0.3 mm. This test is performed to determine the percentage of different grain sizes contained within fly ash. Sieve analysis is performed to determine the distribution of the coarser particles, and the hydrometer method is used to determine the distribution of the finer particles. Testing of these samples follows, as much as practical, the ASTM standards (D422). Figure 3.3 shows the particle size distributions of the fly ash used here comparison with sludge and bentonite. The test method from the ASTM standard (D854) indicates that the fly ash has a specific gravity of 2.67.



(* Wetchasat, 2013)

Figure 3.3 Grain size distribution of fly ash compared with sludge and bentonite results.

The Atterberg's limits are index properties of samples. Depending on the water content of the samples, it may appear in four states solid, semi-solid, plastic and liquid. In each state, the difference of consistency and behavior of sample causes the different engineering properties. The Atterberg limits can be used to distinguish between silt and clay, and it can distinguish between different types of silts and clays. Thus, fly ash has been tested to find these indexes by using the ASTM D4318 and D2487. The results are listed in Table 3.1. The fly ash samples are classified according to the Unified Soil Classification System is in the ML (inorganic silt).

Table 3.1 Atterberg's limits and specific gravity of fly ash, sludge, and bentonite.

Atterberg Limits	Fly Ash (%weight)	Bentonite (%weight)		Sludge (%weight)
	SUT	SUT	US	Wetchasat (2013)
Liquid limit	21	400	478	55
Plastic limit	17	20	28	22
Plasticity index	4	380	449	23
Specific gravity	2.67	2.61	-	2.56

Note: SUT = Suranaree University of Technology Laboratory,

US = Castelbaum and Shackelford (2009)

Fly ash samples from The Electricity Generating Authority of Thailand, Mae Moh power plant contain more than 41 percent silicon dioxide (SiO_2), 18 percent aluminum oxide (Al_2O_3), 17 percent calcium oxide (CaO) and 14 percent iron oxide that chemical composition is determined based on X-ray fluorescence spectrometer

(reported from National Metal and Materials Technology Center, National Science and Technology Development Agency database). X-ray fluorescence (XRF) is used to study the chemical compositions of the materials. The objective of analysis is to determine oxide concentrations in samples with X-ray fluorescence spectrometer, Philips PW-2404. Samples used in this analysis are fly ash and bentonite powders. Test method is semi-quantitative X-ray fluorescence spectrometry analysis. Laboratory conducted here are under $25 \pm 5^\circ\text{C}$ and relative humidity of $60 \pm 10\%$. The sample were mixed with binder ($\text{C}_{38}\text{H}_{76}\text{N}_2\text{O}_2$, sample binder, 4:0.8 by weight). They were pressed to form pellets with 3.2 cm diameter. Results of oxide concentrations in the fly ash samples are shown in Table 3.2, (ASTM C114).

3.3 Bentonite

Bentonite is an engineering material as excellent sealant material because of its low permeability, desirable swelling and self-healing characteristic, sorptive qualities and longevity in nature. Bentonite is used extensively for grouting material to reduce permeability in fractured rock mass. Bentonite mixed with cement is made to hold themselves, and not piping with the water pressure while curing in the rock fractures (Akgün and Daemen, 1999; Fuenkajorn and Daemen, 1996; Svermova et al., 2003; Metcalfe and Walker, 2004). The bentonite is used in this study is from Thai Nippon chemical industry, Thailand. Tables 3.1 and 3.2 summarize the chemical compositions and engineering properties of the bentonite tested in this study.

Table 3.2 Results of oxide concentrations in the bentonite and fly ash samples.

Oxide	Concentration (% weight)			
	Fly ash		Bentonite	
	SUT	Ping, H. et al., (2015)	Wetchasat, (2013)	ACC
Al ₂ O ₃	18.33	36.08	19.85	19.8
SiO ₂	40.72	47.75	61.93	61.3
SO ₃	7.48	0.60	1.27	-
Fe ₂ O ₃	14.40	5.36	4.45	3.9
CaO	16.52	5.72	1.27	0.6
K ₂ O	1.77	1.14	0.44	0.4
TiO ₂	0.50	1.22	0.19	0.1
Cr ₂ O ₃	0.02	-	-	-
MnO ₂	0.14	0.07	-	-
ZnO	0.03	-	-	-
As ₂ O ₅	0.04	-	-	-
Rb ₂ O	0.03	-	-	-
ZrO ₂	0.03	-	0.03	-
Na ₂ O	-	0.66	1.63	2.2
MgO	-	1.02	2.44	1.3
P ₂ O ₅	-	0.15	0.05	-
MnO	-	-	0.02	-
CuO	-	-	0.01	-
SrO	-	-	0.03	-
Y ₂ O ₃	-	-	0.01	-
Ir ₂ O ₃	0.015	-	-	-
BaO	-	-	0.03	-
CeO ₂	-	-	0.04	-
LOI. at 1,025 °C	-	-	6.29	-
Total	100	-	100	-

Note: SUT = Suranaree University of Technology Laboratory,

ACC = American Colloid Company Technical Data

3.4 Portland cement

Portland cement type I is used in conforms to the ASTM C150. Portland cement can be purchased readily, low cost and widely used in the construction. Portland cement of INSEE dang brand, bag cement 50 kg, used in this study is from

the Siam City Cement Public Company (SCCC) Limited, Thailand. The cement is kept in plastic box sealed to prevent moisture, cool-dry area.

Portland cement of INSEE dang brand conforms to the ASTM C91 standard which is autoclave expansion of 0.001%, setting time (by Gillmore Method) for initial of 145 minutes and final of 245 minutes. The mortar compressive strength for 7 and 28 days is 13 and 15.5 MPa. The amount of air content in mortar is 15.5%, with water retention value of 78.5% (percentage of original flow). Table 3.3 summaries the chemical compositions of Portland cement type I, which is the same type used in this study, (Ali, 2008).

Table 3.3 Results of oxide concentrations in Portland cement (Ali, 2008).

Silicon dioxide (SiO ₂)	20.58
Aluminum oxide (Al ₂ O ₃)	5.71
Ferric oxide (Fe ₂ O ₃)	2.94
Calcium oxide (CaO)	64.76
Magnesium oxide (MgO)	0.87
Potassium oxide (K ₂ O)	0.67
Sulfer trioxide (SO ₃)	2.63
Sodium oxide (Na ₂ O)	0.14
Titanium Oxide (TiO ₂)	0.29
Phosphorus oxide (P ₂ O ₅)	0.06
Loss on ignition (LOI)	0.96

3.5 Rock samples

The selection criteria for rock sample are that the rock should be homogeneous and availability as much as possible. This is to minimize the intrinsic variability of the test results. The sandstone samples are used and collected from Phu Kradung formation. Sample preparations are carried out in the Geomechanics Research (GMR) laboratory facility at Suranaree University of Technology. Sample preparations have been carried out for series for constant head flow testing (Figure 3.4) and direct shear test (Figure 3.5).

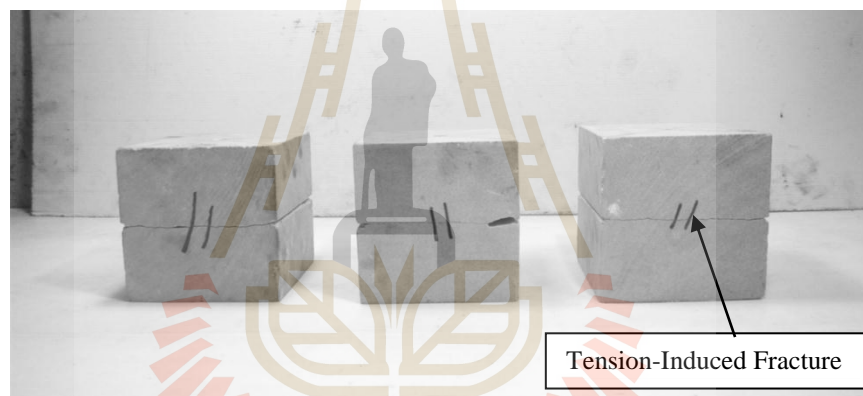


Figure 3.4 Some sandstone samples with $130 \times 130 \times 130 \text{ mm}^3$ prismatic blocks for series for constant head flow testing.

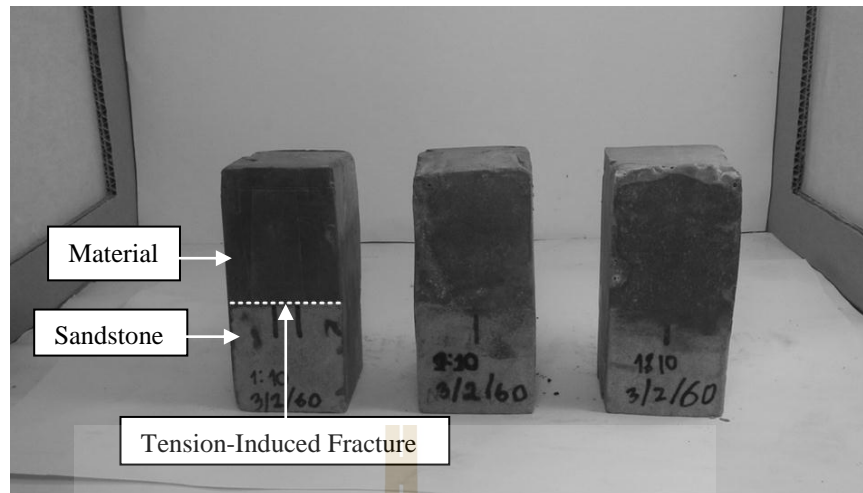


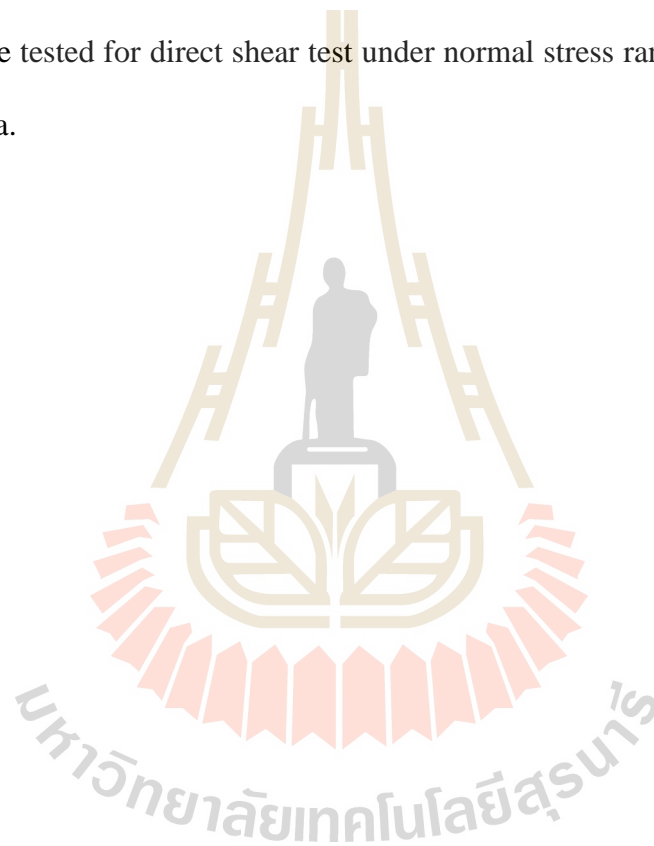
Figure 3.5 Some specimen samples with a width, length dimension of 54 mm and 108 mm of high for direct shear testing.

3.5.1 Sample preparation for constant head flow test under various normal stresses

Sandstone samples for the constant head test are prepared to have prismatic blocks of sandstone. Preparation of these samples follows the suggested methods proposed by Navarro (2010). The fractures are artificially made by applying a line load at the center to induce a splitting tensile crack in $130 \times 130 \times 130 \text{ mm}^3$ prismatic blocks. The fracture area is $130 \times 130 \text{ mm}^2$. The injection hole at the center of the upper block is 10 mm in diameter. A minimum of twenty sandstone specimens are tested for constant head flow test with both three portions of fly ash-mixed cement and bentonite-mixed cement under normal stress ranging from 0.25, 0.75, and 1.25 MPa.

3.5.2 Sample preparation for direct shear test under various normal stresses

Preparation of sandstone specimens follows the ASTM standards D4543 with a width dimension of 54 mm and 108 mm of length. The fractures are artificially made by applying a line load at the center of length to induce a splitting tensile crack. The fracture area is 2,916 mm². A minimum of twelve sandstone specimens are tested for direct shear test under normal stress ranging from 0.25, 0.75, and 1.25 MPa.



CHAPTER IV

GROUT PREPARATIONS

4.1 Introduction

This chapter describes the methods and results of laboratory experiments used to determine the most suitable mixing ratios for grouting in rock fracture.

4.2 Viscosity and density of mixtures

The objectives of these tests are to determine proportioning of mixtures and methods to be used to test the mechanical and hydraulic properties in the next step. These results lead to the determination that the most suitable mixing ratios of fly ash-mixed cement should be proportional for grouting in rock fracture. Viscosity measurement follows, as much as practical, the ASTM standard (D2196). Apparatus used in these experiments consist of:

- 1) Fly ash (Figure 4.1),
- 2) Bentonite (Figure 4.2),
- 3) Portland cement (Figure 4.3),
- 4) Distilled water,
- 5) Digital balance with maximum capacity of 2,000 g and accuracy to ± 0.01 g. (Figure 4.4),
- 6) Mixer, Kitch enaid Professional 600 6QT 575 watt stand mixer, with maximum capacity of 5,000 cm³ and 6 speed control (Figure 4.5),

- 7) Brookfield Viscometer (Rheometers) RV 203 Watt 50 Hz (Figure 4.6), and
- 8) Laser thermometer TAITAN T350C with range $-50 \sim 350^{\circ}\text{C}$ (Figure 4.7).



Figure 4.1 Fly ash from The Electricity Generating Authority of Thailand, Mae Moh power plant used in this study.



Figure 4.2 Thai Nippon chemical industry bentonite used in this study.



Figure 4.3 Bag of Portland cement 50 kg is used in this study.



Figure 4.4 Digital balance with maximum capacity for 2000 grams and accuracy to ± 0.01 gram.



Figure 4.5 Mixer, Kitchenaid Professional 600 6QT 575 watt stand mixer, with maximum capacity for 5,000 cm³ and 6 speed control.



Figure 4.6 Viscometer, Bookfield viscometer RV 203 Watt 50 Hz.

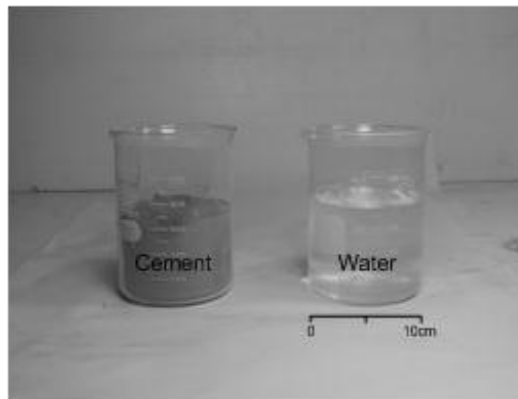


Figure 4.7 Laser thermometers TAITAN T350C with range $-50 \sim 350^{\circ}\text{C}$.

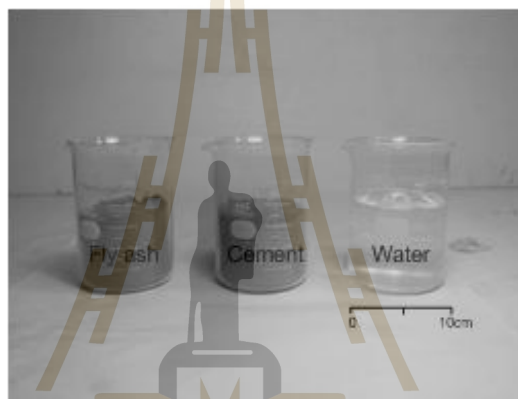
4.2.1 Test methods

The preliminary selection in proportions of mixtures including fly ash (F), bentonite (B), Portland cement (C), and distilled water (W) are determined and given by using viscosity values. Proportions of the mixtures are shown in Table 4.1. Test procedure also follows:

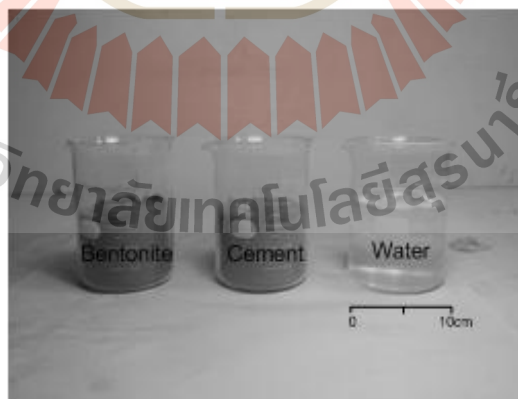
- 1) Material balance of the four types defined, the proportion in the beaker for tests (Figure 4.8).
- 2) The material is weighed and then put together in a plastic bag and tie tightly. Make a homogeneous mixture by shaking several times.
- 3) Pour the distilled water into the bag to weigh it down and turn the mixer speed up to 275 rpm. Mixing of all grouts is accomplished using a blade paddle mixer as suggested in ASTM standard C938.



(a)



(b)



(c)

Figure 4.8 Grouting materials in beakers are prepared for mix proportion (a) cement and water, (b) cement, water and fly ash, and (c) cement, water and bentonite.

4) Pour the mixed material in Section 2 into the mix to run at the same time. If there is additional material should be poured within a two-minute timer and start pouring the mixture into distilled water. Measure the room temperature by laser thermometer.

5) In a homogeneous mix for 3 minutes to complete mixing at 275 rpm, then turn off the mixer.

6) Determine the density and viscosity of the mixture slurry by using standard ASTM standard (D2196). Pour in a beaker with a volume of the mixture is equal to exactly 500 cc (Figure 4.9).

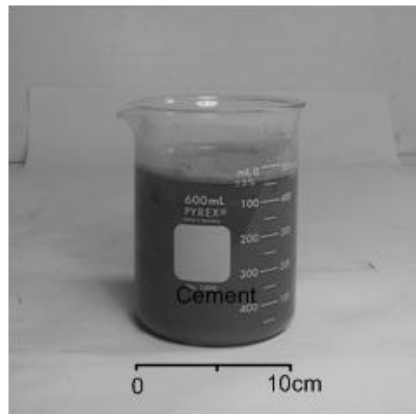
7) Weigh the beaker with the mixture. Subtract the weight of the beaker from the results and then divided by the volume of the mixture (500 cc) is the density of mixture slurry.

8) Specific gravity (SG) of the mixture is calculated from equation

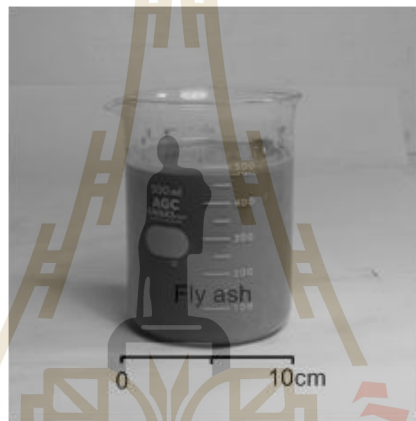
$$SG = \rho_{\text{slurry}} / \rho_w \quad (4.1)$$

where ρ_{slurry} is a density of mixture slurry, and ρ_w is density of distilled water at the time of measurement. The results of the test density and specific gravity are summarized in Table 4.1.

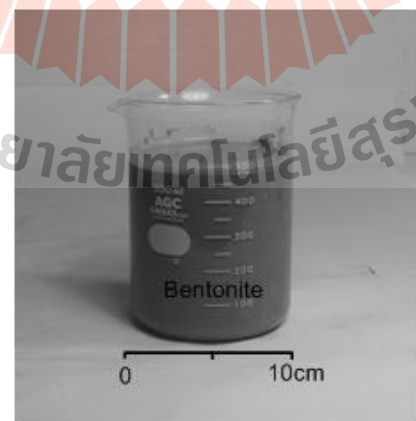
Viscosity test is performed after the weighing of ingredients in the measuring beaker with a volume of 500 cc, which is continuing immediately. The viscosity of the mixture, which is resistant to flow, can be determined by a rotational viscometer, Brookfield model RV dial reading viscometer. Spindle set (RV-1 through RV-7) is selected for this test. Testing of viscosity follows the ASTM standard D2196.



(a)



(b)



(c)

Figure 4.9 Slurry volume of 500 cc in beakers for the density and viscosity tests (a) cement paste (b) fly ash-cement slurry, and (c) bentonite-cement slurry.

1) For the mixture of given viscosity, the resistance is greater as the spindle size and rotational speed increase. The minimum viscosity ranged, is obtained by using the largest spindle at the highest speed; the maximum range by using the smallest spindle at the slowest speed.

2) The sample is placed in Glass Beaker (500 cm³) under viscometer (Figure 4.10).

Table 4.1 Results of slurry density tests in beakers of 500 cc.

Binder	F:C:W or B:C:W	T _{Slurry} (°C)	W _{Slurry} (g)	ρ _{Slurry} (g/cc)	ρ _{Water} (g/cc)	SG
Cement	0:10:10	26.5	729.21	1.46	0.996	1.47
Fly ash	1:10:10	28.4	769.75	1.54	0.996	1.55
	3:10:10	27.5	796.13	1.59	0.996	1.60
	5:10:10	27.0	831.26	1.66	0.996	1.67
	6:10:10	26.6	838.82	1.68	0.997	1.69
	7:10:10	26.5	849.41	1.70	0.996	1.71
	8:10:10	26.5	855.50	1.71	0.997	1.72
	9:10:10	26.2	869.01	1.74	0.997	1.75
	10:10:10	26.4	873.33	1.75	0.997	1.76
	15:10:10	26.4	888.83	1.78	0.997	1.79
Bentonite	1:10:10	27.0	761.90	1.52	0.996	1.53
	2:10:10	28.0	820.21	1.64	0.996	1.65
	3:10:10	28.0	824.31	1.65	0.996	1.65
Sludge (Wetchasat, 2013)	1:10:10	28.6	733.51	1.47	0.996	1.47
	3:10:10	30.2	742.02	1.48	0.996	1.49
	5:10:10	30.3	794.50	1.59	0.996	1.60

3) Weight and temperature of each sample are recorded to determine a slurry density.

4) Releasing the brake once the viscometer is rotating smoothly and time for 60 seconds. Brake firmly is depressed and the viscometer is turned off during continuing to hold the brake down. Values on the viscometer gauge are read and recorded. Recording the number of the spindles is used.

5) Calculating the viscosity in centipoises by multiplying the meter reading by the multiplier corresponding to the particular spindle used.

The reading of the test Viscosity Brookfield is in units of centipoise (cP) or equal mPa·s in dynamic viscosity. The dynamic viscosity is converted to the kinetic viscosity by equation (4.2).

$$\mu = \rho \cdot \nu \quad (4.2)$$

where μ is dynamic viscosity, ν is the kinetic viscosity, and ρ is slurry density.

4.2.2 Test results

Figure 4.11 shows kinematic viscosity of bentonite-cement and fly ash-cement mixtures for different ratios. At W:C ratio equal to one. The test results of slurry density tests in beakers of 500 cc. The results of slurry viscosity tests are listed in Table 4.2.

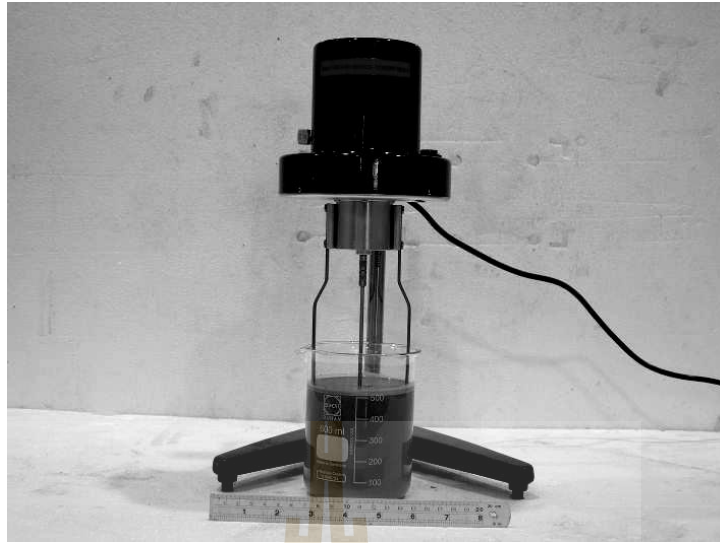
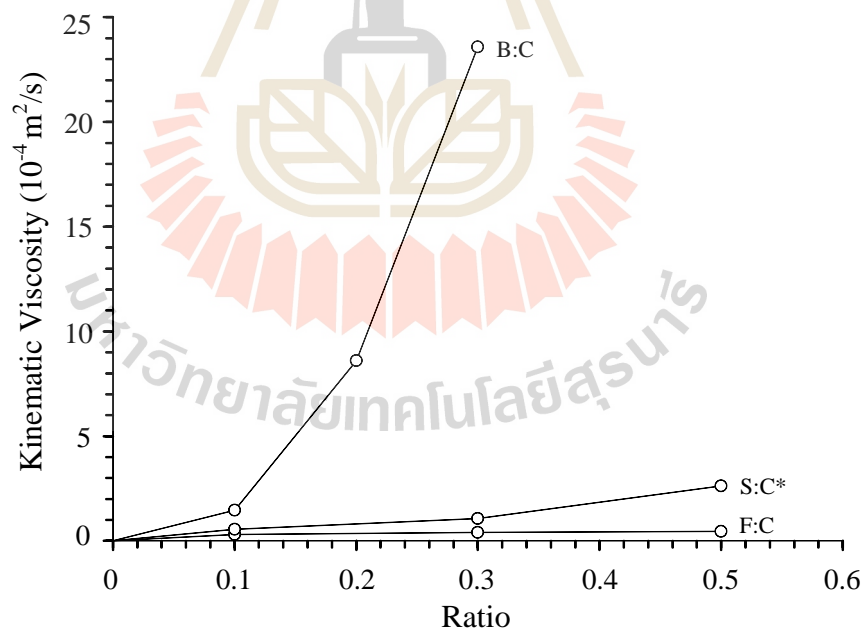


Figure 4.10 Brookfield model RV dial reading viscometer is used for viscosity and slurry density tests.



*(Wetchasat, 2013)

Figure 4.11 Kinematic viscosity of bentonite-cement, sludge-cement and fly ash-cement mixtures for different W:C ratios.

Table 4.2 Results of slurry viscosity tests in beakers of 500 cc.

Binder	F:C:W or B:C:W	Temperature (°C)			ρ^{Slurry} (g/cc)	Dynamic Viscosity (Pa·s)	Kinematic Viscosity ($10^{-3} \text{ m}^2/\text{s}$)
		Air	Water	Slurry			
Cement	0:10:10	27.3	26.5	26.5	1.46	3.39	0.23
Fly ash	1:10:10	28.5	28.0	28.4	1.54	4.73	0.31
	3:10:10	27.7	27.5	27.5	1.59	6.51	0.41
	5:10:10	27.7	27.8	27.0	1.66	7.60	0.46
	6:10:10	26.5	26.4	26.6	1.68	11.00	0.66
	7:10:10	26.4	26.5	26.5	1.70	20.00	1.18
	8:10:10	26.5	26.6	26.5	1.71	29.00	1.70
	9:10:10	26.3	26.5	26.2	1.74	56.00	3.22
	10:10:10	26.5	26.4	26.4	1.75	68.00	3.89
	15:10:10	26.4	26.4	26.4	1.78	122.00	6.86
	20:10:10	26.4	26.3	26.3	1.80	292.00	16.22
Bentonite	1:10:10	27.1	27.5	27.0	1.52	22.25	1.46
	2:10:10	27.5	27.5	28.0	1.64	141.00	8.60
	3:10:10	28.0	27.5	28.0	1.65	389.00	23.58
Sludge (Wetchasat, 2013)	1:10:10	31.3	27.5	28.6	1.47	8.17	0.56
	3:10:10	32.3	27.5	30.2	1.48	15.75	1.06
	5:10:10	31.5	27.5	30.3	1.59	41.72	2.63

CHAPTER V

MECHANICAL PROPERTIES TESTING

5.1 Introduction

This chapter describes the methods and results of laboratory tests used to determine the compressive strength for the six proportions of grouting materials selected from Chapter IV. Pure cement is tested in terms of mechanical properties. Preparation of these samples follows, as much as practicable, the ASTM standards ASTM C150. Direct shear testing is performed to determine the shear resistance occurs at the interface between the surfaces of grouting material and fractured sandstone.

5.2 Basic Mechanical Properties Tests of Cement Grout

The basic mechanical properties tests of cement grout include Uniaxial compressive strength (σ_c), Elastic modulus (E), Brazilian tensile strength (σ_B), Bond strength (τ_{av}), and Shear strength (τ). Summary of parameters and results for basic mechanical testing are listed in Table 5.1-5.4.

5.2.1 Uniaxial compressive strength testing.

The objectives of the uniaxial compressive strength tests are, 1) to evaluate the basic mechanical properties of grouting material specimens of 54 mm in diameter at three curing times. They are out of the mold and cut to L/D ratio of about 2–2.5 (Figure 5.1). They are used as an index to confirm that the proportions of



Figure 5.1 Core sample is cut to obtain the desired length with Husqvarna Construction Products 433-81 Gothenburg Sweden.

F:C:W and B:C:W mixtures are appropriate selection of the viscosity of mixture slurry from Chapter IV, and 2) to determine the uniaxial compressive strength (σ_c), Poisson's ratio (ν), and elastic modulus (E) of grouting material specimens of 54 mm in diameter cylindrical specimens with length to diameter ratios between 2.0 to 2.5 are prepared by curing cement pastes in PVC molds for 3, 7, 14, and 28 days. The specimens are tested with a loading rate of 1 MPa/s for the uniaxial compressive strength test (Figure 5.2). During the test, the failure modes are monitored (Figure 5.3). The mixtures from the preparation (in Chapter IV) and the results from initially uniaxial compressive strength test are used for selected suitable mixing ratios. The suitable mixing ratios for the F:C:W mixtures are 1:10:10, 3:10:10, 5:10:10 and for the B:C:W mixtures are 1:10:10, 2:10:10, 3:10:10 by weight. This is a part of the material characterization. The material parameters are sample size, weight, density, failure load, and mode of failure, etc. And parameters are monitored, recorded and analyzed.

Table 5.1 Summary of parameters and results for basic mechanical of Uniaxial compressive testing at curing time 3 days.

Types	Sample no.	L (mm)	D (mm)	L/D	W (g)	ρ (g/cc)
B:C:W = 0:10:10	C-01	135.60	54.00	2.51	483.62	1.56
	C-02	128.10	54.65	2.34	475.60	1.58
	C-03	135.25	54.15	2.50	492.02	1.58
	C-04	135.50	54.00	2.51	483.44	1.56
	C-05	136.85	53.80	2.54	496.22	1.59
B:C:W = 1:10:10	BC1-01	136.35	54.25	2.51	501.10	1.59
	BC1-02	139.30	55.80	2.50	556.92	1.63
	BC1-03	141.70	56.00	2.53	562.33	1.61
	BC1-04	137.00	53.80	2.55	501.92	1.61
	BC1-05	136.50	54.00	2.53	497.84	1.59
B:C:W = 2:10:10	BC2-01	134.90	53.50	2.52	479.41	1.58
	BC2-02	136.10	53.80	2.53	494.23	1.60
	BC2-03	135.20	54.00	2.50	491.22	1.59
	BC2-04	140.90	55.60	2.53	552.94	1.62
	BC2-05	135.00	54.00	2.50	480.83	1.56
B:C:W = 3:10:10	BC3-01	142.10	55.70	2.55	563.32	1.63
	BC3-02	144.00	56.30	2.56	567.94	1.58
	BC3-03	136.00	53.60	2.54	496.02	1.62
	BC3-04	136.35	53.60	2.54	492.75	1.60
	BC3-05	136.00	54.80	2.48	502.50	1.57

Table 5.1 Summary of parameters and results for basic mechanical of Uniaxial compressive testing at curing time 3 days (continued).

Types	Sample no.	L (mm)	D (mm)	L/D	W (g)	ρ (g/cc)
F:C:W = 1:10:10	FC1-01	135.70	53.40	2.54	513.22	1.69
	FC1-02	137.70	56.60	2.43	561.74	1.62
	FC1-03	140.25	56.00	2.50	571.20	1.65
	FC1-04	127.10	56.25	2.26	510.94	1.62
	FC1-05	139.40	57.00	2.45	559.50	1.57
F:C:W = 3:10:10	FC3-01	140.50	56.60	2.48	589.72	1.67
	FC3-02	140.25	56.35	2.49	581.81	1.66
	FC3-03	137.63	53.90	2.55	515.30	1.64
	FC3-04	141.60	56.60	2.50	580.44	1.63
	FC3-05	135.50	56.35	2.40	559.00	1.65
F:C:W = 5:10:10	FC5-01	138.00	53.70	2.57	503.22	1.61
	FC5-02	140.75	56.60	2.49	564.25	1.59
	FC5-03	140.75	56.25	2.50	566.11	1.62
	FC5-04	139.60	56.40	2.48	559.00	1.60
	FC5-05	141.60	56.00	2.53	562.41	1.61

Table 5.2 Summary of parameters and results for basic mechanical of Brazilian tensile testing at curing time 3 days.

Types	Sample no.	L (mm)	D (mm)	L/D	W (g)	ρ (g/cc)
B:C:W = 0:10:10	C-01	26.70	53.00	0.50	94.00	1.60
	C-02	26.85	54.25	0.49	97.10	1.56
	C-03	27.40	53.30	0.51	99.00	1.62
	C-04	27.35	56.60	0.48	100.10	1.45
	C-05	26.85	53.50	0.50	97.90	1.62
B:C:W = 1:10:10	BC1-01	27.70	53.70	0.52	102.10	1.63
	BC1-02	28.00	53.70	0.52	97.30	1.53
	BC1-03	27.40	53.90	0.51	104.90	1.68
	BC1-04	28.20	53.80	0.52	105.20	1.64
	BC1-05	27.90	54.00	0.52	100.10	1.57
B:C:W = 2:10:10	BC2-01	27.80	53.80	0.52	98.00	1.55
	BC2-02	27.80	53.70	0.52	97.70	1.55
	BC2-03	28.10	54.00	0.52	100.10	1.56
	BC2-04	27.00	54.00	0.50	96.20	1.56
	BC2-05	28.80	53.80	0.54	102.20	1.56
B:C:W = 3:10:10	BC3-01	27.70	53.70	0.52	98.40	1.57
	BC3-02	26.80	53.50	0.50	95.60	1.59
	BC3-03	28.00	53.50	0.52	100.00	1.59
	BC3-04	28.10	53.30	0.53	101.20	1.61
	BC3-05	27.8	53.80	0.52	99.70	1.58

Table 5.2 Summary of parameters and results for basic mechanical of Brazilian tensile testing at curing time 3 days (continued).

Types	Sample no.	L (mm)	D (mm)	L/D	W (g)	ρ (g/cc)
F:C:W = 1:10:10	FC1-01	28.00	54.50	0.51	96.20	1.47
	FC1-02	27.20	54.00	0.50	98.30	1.58
	FC1-03	27.40	54.30	0.50	102.60	1.62
	FC1-04	26.60	54.40	0.49	101.80	1.65
	FC1-05	27.50	53.30	0.52	100.90	1.64
F:C:W = 3:10:10	FC3-01	27.60	54.40	0.51	104.10	1.62
	FC3-02	27.20	54.20	0.50	104.60	1.67
	FC3-03	27.10	54.30	0.50	101.10	1.61
	FC3-04	27.20	53.70	0.51	106.10	1.72
	FC3-05	27.00	54.00	0.50	96.30	1.56
F:C:W = 5:10:10	FC5-01	27.80	54.00	0.51	101.60	1.60
	FC5-02	28.60	54.00	0.53	104.30	1.59
	FC5-03	28.10	53.80	0.52	100.50	1.57
	FC5-04	27.80	53.90	0.52	100.50	1.58
	FC5-05	28.30	54.00	0.52	102.70	1.58

Table 5.3 Summary of parameters and results for basic mechanical of push out testing at curing time 3 days.

Types	Sample no.	Sandstone specimen (W×L×H, mm)	L (mm)	D (mm)	L/D	W (g)	ρ (g/cc)
F:C:W = 0:10:10	C-01	130×131×130	85.00	45.00	1.89	210.89	1.56
	C-02	129×131×130	85.00	45.00	1.89	212.24	1.57
	C-03	130×130×131	90.00	45.00	2.00	229.02	1.60
	C-04	132×131×129	90.00	45.00	2.00	229.02	1.60
	C-05	130×130×129	87.00	45.00	1.93	221.39	1.60
F:C:W = 1:10:10	FC1-01	129×129×131	95.00	45.00	2.11	243.26	1.61
	FC1-02	131×131×130	90.00	45.00	2.00	226.16	1.58
	FC1-03	130×130×130	90.00	45.00	2.00	227.59	1.59
	FC1-04	129×131×130	90.00	45.00	2.00	230.45	1.61
	FC1-05	129×129×131	90.00	45.00	2.00	230.45	1.61
F:C:W = 3:10:10	FC3-01	131×129×130	95.00	45.00	2.00	244.77	1.62
	FC3-02	130×131×131	90.00	45.00	2.00	231.88	1.62
	FC3-03	130×130×131	90.00	45.00	2.00	231.88	1.62
	FC3-04	131×131×131	90.00	45.00	2.00	233.32	1.63
	FC3-05	129×129×130	90.00	45.00	2.00	229.02	1.60
F:C:W = 5:10:10	FC5-01	131×131×129	85.00	45.00	1.89	213.59	1.58
	FC5-02	130×130×131	85.00	45.00	1.89	212.24	1.57
	FC5-03	130×131×130	87.00	45.00	1.93	221.39	1.60
	FC5-04	131×131×130	90.00	45.00	2.00	231.88	1.62
	FC5-05	130×129×129	90.00	45.00	2.00	229.02	1.60

Table 5.4 Summary of parameters and results for basic mechanical of direct shear testing at curing time 3 days.

Types	Sample no.	Specimen (W×L×H, mm)	Cross section area (mm ²)
F:C:W = 0:10:10	C-01	54×54×108	2916
	C-02	54×54×108	2916
	C-03	53×54×109	2826
F:C:W = 1:10:10	FC1-01	54×53×108	2826
	FC1-02	53×53×109	2809
	FC1-03	54×54×108	2916
F:C:W = 3:10:10	FC3-01	53×54×109	2826
	FC3-02	53×53×109	2809
	FC3-03	54×53×108	2826
F:C:W = 5:10:10	FC5-01	53×55×107	2915
	FC5-02	54×54×108	2916
	FC5-03	54×55×108	2970

The suitable mixing ratios for the F:C:W and B:C:W mixtures are selected and compared.

Preparation of these samples follows, as much as practical, the ASTM D7012, C938 and C39, 2) are tested under water at room temperature (ASTM standard C192).

The failure stress is calculated by dividing the axial load by the cross-section area of specimen. The compressive strength (σ_c) is determined from the maximum load (P_f) divided by the original cross-section area (A):

$$\sigma_c = P_f/A \quad (5.1)$$

The results of uniaxial compressive strength test, elastic modulus, and Poisson's Ratio measurements are shown in Table 5.2. Figures 5.4 and 5.5 show the uniaxial compressive strength and elastic modulus as a function of curing time. The curing time increases with the uniaxial compressive strength and elastic modulus of cement grout increasing.

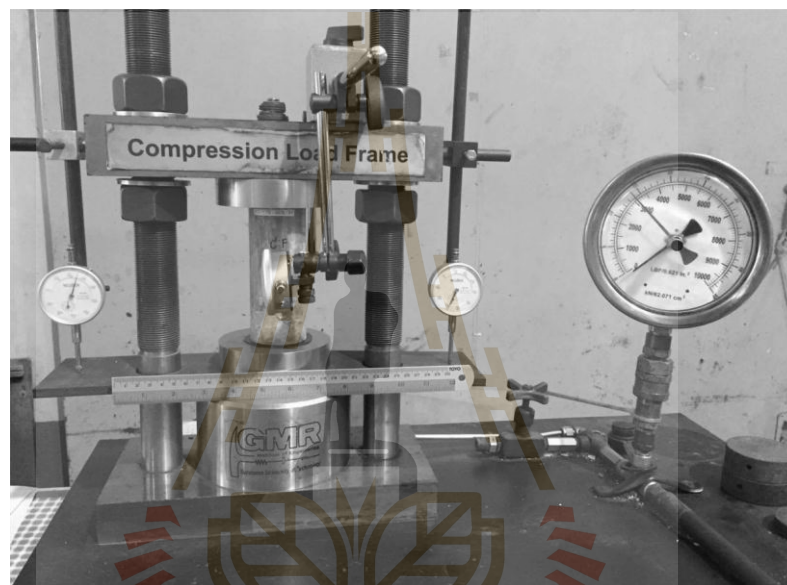
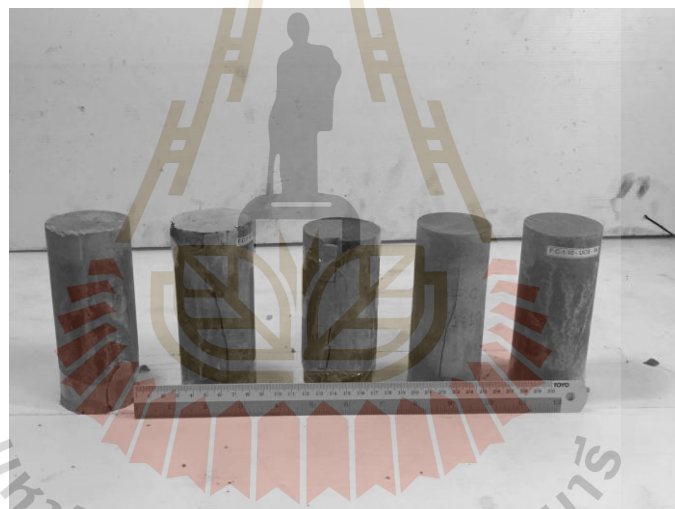


Figure 5.2 Uniaxial compressive strength test with constant loading rate. The cylindrical specimen is loaded vertically using the compression machine.



(a)



(b)

Figure 5.3 Some specimens prepared for basic mechanical testing (a) before testing, and (b) after testing.

Table 5.5 Summary of uniaxial compressive strength, Elastic Modulus, and Poisson's Ratio results on the F:C:W and B:C:W mixtures specimens of 54.00 mm of diameter.

Binder	Curing Time (days)	F:C:W or B:C:W Samples	UCS (MPa)	E (GPa)	ν
Fly ash	3	1:10:10	2.62 ± 0.19	0.57 ± 0.02	0.13 ± 0.02
		3:10:10	3.28 ± 0.34	0.61 ± 0.08	0.14 ± 0.01
		5:10:10	3.33 ± 0.25	0.66 ± 0.10	0.17 ± 0.00
	7	1:10:10	3.27 ± 0.40	0.60 ± 0.07	0.22 ± 0.04
		3:10:10	5.35 ± 0.23	0.64 ± 0.05	0.16 ± 0.03
		5:10:10	6.33 ± 0.77	0.75 ± 0.03	0.10 ± 0.03
	14	1:10:10	5.36 ± 0.69	0.78 ± 0.10	0.14 ± 0.03
		3:10:10	6.93 ± 0.30	0.85 ± 0.08	0.12 ± 0.02
		5:10:10	7.83 ± 1.19	1.12 ± 0.05	0.17 ± 0.02
	28	1:10:10	6.10 ± 1.01	0.95 ± 0.06	0.09 ± 0.02
		3:10:10	7.16 ± 0.31	1.12 ± 0.12	0.21 ± 0.04
		5:10:10	10.45 ± 1.48	1.36 ± 0.05	0.12 ± 0.03
Bentonite	3	1:10:10	3.08 ± 0.41	0.58 ± 0.04	0.08 ± 0.01
		2:10:10	3.64 ± 0.18	0.58 ± 0.04	0.09 ± 0.03
		3:10:10	3.22 ± 0.40	0.48 ± 0.15	0.14 ± 0.02
	7	1:10:10	3.75 ± 0.38	0.78 ± 0.02	0.15 ± 0.06
		2:10:10	4.08 ± 0.12	0.64 ± 0.10	0.14 ± 0.03
		3:10:10	3.81 ± 0.36	0.58 ± 0.03	0.17 ± 0.02
	14	1:10:10	5.03 ± 0.23	0.88 ± 0.11	0.15 ± 0.06
		2:10:10	5.27 ± 0.28	0.79 ± 0.13	0.20 ± 0.03
		3:10:10	4.58 ± 0.30	0.67 ± 0.10	0.08 ± 0.02
	28	1:10:10	5.27 ± 0.62	1.07 ± 0.07	0.15 ± 0.05
		2:10:10	5.89 ± 0.26	0.81 ± 0.06	0.21 ± 0.04
		3:10:10	5.52 ± 0.86	0.77 ± 0.02	0.16 ± 0.02
Cement	3	0:10:10	1.91 ± 0.23	0.44 ± 0.03	0.16 ± 0.04
	7	0:10:10	2.99 ± 0.38	0.50 ± 0.03	0.15 ± 0.03
	14	0:10:10	3.27 ± 0.24	0.61 ± 0.04	0.12 ± 0.03
	28	0:10:10	5.21 ± 0.71	0.71 ± 0.05	0.15 ± 0.03

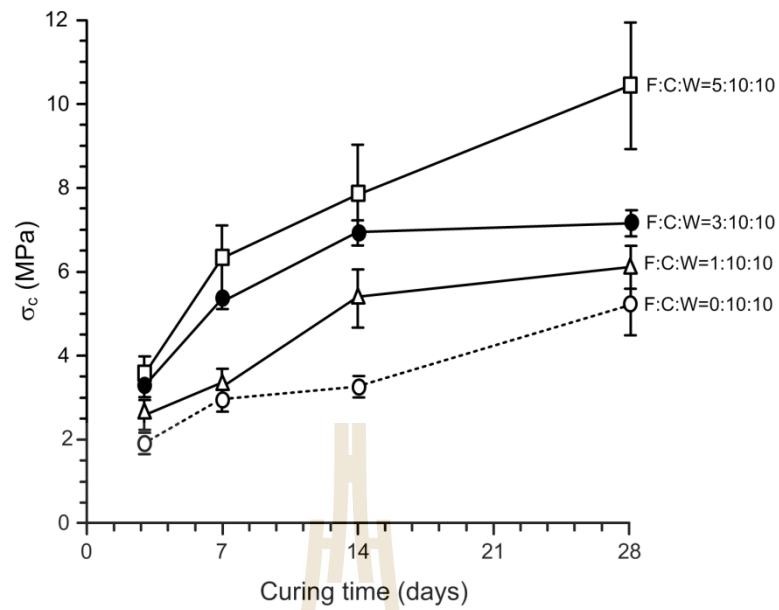


Figure 5.4 Uniaxial compressive strengths fly ash-mixed cement as a function of curing time.

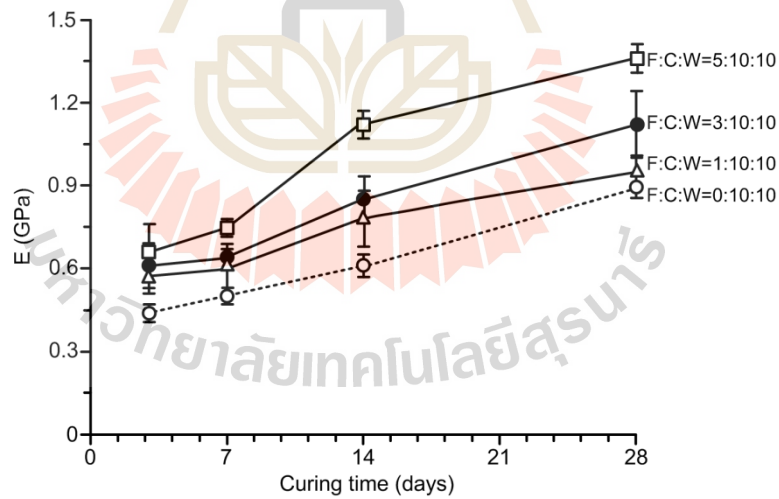


Figure 5.5 Elastic modulus fly ash-mixed cement as a function of curing time.

5.2.2 Brazilian tensile strength tests

The objective of the Brazilian tensile strength tests is to determine the indirect tensile strength of cement grouts. The Brazilian tensile strength tests are performed in accordance with ASTM standard (D3967) and ISRM suggested method (Brown, 1981). Specimens of 54 mm diameter cylindrical cement specimens with length to diameter ratios is 0.5 are prepared by curing cement pastes in PVC molds for 3, 7, 14, 21, and 28 days. The test is performed by increasing the axial loaded at the constant rate of 0.1-0.5 MPa/s to cement grout specimen until failure occurred and some specimens prepared for test (Figures 5.6 and 5.7). At the failure, the tensile strength of the rock is calculated as follows.

$$\sigma_B = 2P / \pi Dt \quad (5.2)$$

where P is applied load (N), D is diameter of the sample (mm), t is thickness of the sample (mm). The average splitting tensile strength after 28 days is 1.91 MPa.



Figure 5.6 Brazilian tensile strength test with constant loading rate.

The results of Brazilian tensile strength tests are shown in Table 5.3.

Figure 5.8 shows the Brazilian tensile strength as a function of curing time. The curing time increases the Brazilian tensile strength of cement grout increases.



Figure 5.7 Some specimens prepared for Brazilian tensile strength testing

Table 5.6 Summary of Brazilian tensile strength test results on the F:C:W and B:C:W mixtures specimens.

Binder	F:C:W or B:C:W Samples	Tensile strength (MPa)			
		Curing Time (days)			
		3	7	14	28
Fly ash	0:10:10	0.79 ± 0.14	1.21 ± 0.26	1.47 ± 0.14	1.51 ± 0.12
	1:10:10	1.03 ± 0.24	1.23 ± 0.23	1.52 ± 0.07	1.81 ± 0.09
	3:10:10	1.12 ± 0.17	1.49 ± 0.12	1.63 ± 0.11	1.85 ± 0.32
	5:10:10	1.22 ± 0.09	1.52 ± 0.10	1.72 ± 0.05	1.91 ± 0.01
Bentonite	1:10:10	1.36 ± 0.13	1.37 ± 0.15	1.39 ± 0.21	1.44 ± 0.05
	2:10:10	1.04 ± 0.12	1.12 ± 0.04	1.12 ± 0.14	1.14 ± 0.06
	3:10:10	1.00 ± 0.11	1.02 ± 0.02	1.05 ± 0.14	1.08 ± 0.21

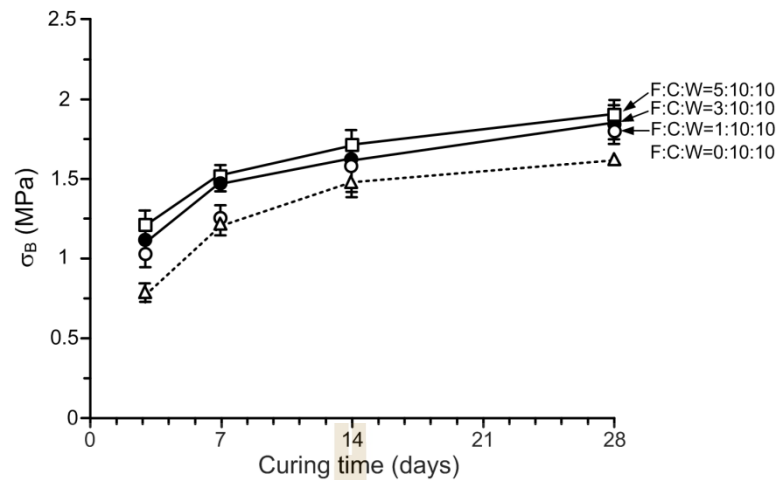


Figure 5.8 Brazilian tensile strength fly ash-mixed cement as a function of curing time.

5.2.3 Push-out test

The objective of this test is to determine the axial mechanical strength or bond strength of cement grout casted in a hole at the center of the specimen with a diameter of 45 mm and length of 90 mm. The cement grouts casted in the hole at the center of Phu Kradung sandstone are axially loaded at the constant rate of 0.1-0.5 MPa/s until sliding occurs. The curing period for push-out tests are 3, 7, 14, and 28 days. Figure 5.9 shows the schematic drawing of the push-out test setup. A cylindrical steel rod applies an axial load to a cement plug. The top and bottom displacement of the borehole plug are measured by dial gages. The figure 5.10 shows the sample for test. The axial load is measured by a load gage of hydraulic pump. The displacement is measured manually by dial gages with a resolution of 0.025 mm. A loading frame with a hydraulic cylinder applies the load. The machine has a capacity of 50 kN with a resolution of 0.5 kN. The strength is calculated by:

$$\tau_{av} = P/\pi DL \quad (5.3)$$

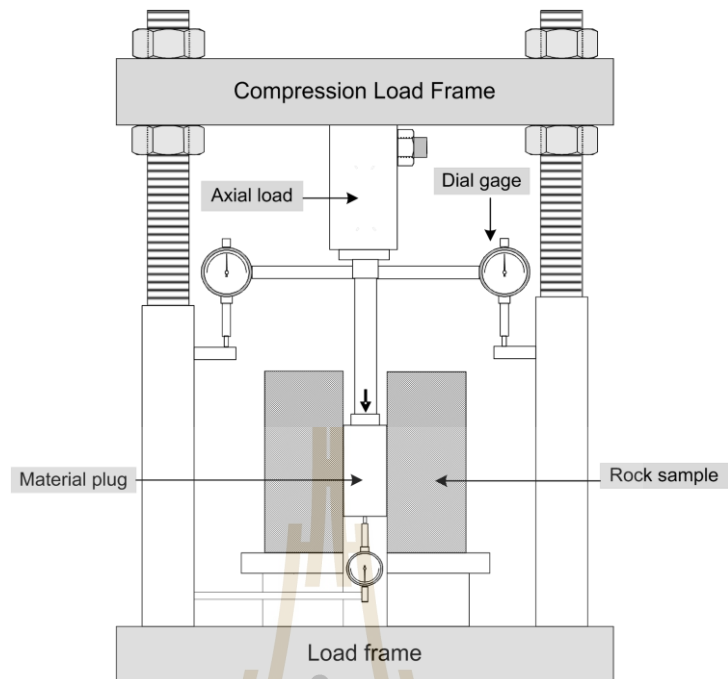
where P is the failure load, D is the plug diameter and L is the plug length.

The results of Put-out tests are shown in Table 5.7. Figure 5.11 shows the bond strength as a function of curing time. The curing time increases the bond strength of cement grout increasing.

5.2.4 Shearing resistance between grout and fracture

The objective of the fracture shear test is to determine the direct shear strength of grouting material in sandstone fracture. Grouting materials are fly ash-mixed cement. The experimental procedure is similar to the ASTM standard (D5607). The constant normal stresses are 0.25, 0.75, and 1.25 MPa. The shear stresses are applied while the shear displacement and head drop are monitored for every 0.2 mm of shear displacement. Similarities and differences of the results are compared. The mixtures from the preparation in Chapter IV and the results from tasks 5.2 are used for selected suitable mixing ratios.

Proportions of F:C:W mixtures are 0:10:10, 1:10:10, 3:10:10, and 5:10:10 by weight. Preparation of these samples follows, as much as practical, the ASTM C938. The molded of with a width dimension of 54 mm and 108 mm of length. The fractures are artificially made by applying a line load at the center of length to induce splitting tensile crack. The shear strength tested is carried out at the ages of 7 days curing. Laboratory arrangement for the direct shear test equipment is shown in Figure 5.12. The constant normal stresses used, are 0.25, 0.75, and 1.25 MPa. The shear stresses, is applied while the shear displacement and dilation are monitored for every 0.2 mm of shear displacement.



(a)



(b)

Figure 5.9 Bond strength testing.(a) the schematic drawing of the push-out test, and (b) push-out test setup.

Table 5.7 Summary of push-out test average shear strength test results on the F:C:W mixtures specimens.

Curing Time (days)	Average shear strength (MPa)			
	F:C:W			
	0:10:10	1:10:10	3:10:10	5:10:10
3	0.22	0.25	0.26	0.36
7	0.63	0.67	0.94	1.45
14	0.65	0.94	1.07	1.69
28	0.67	1.12	1.20	2.23

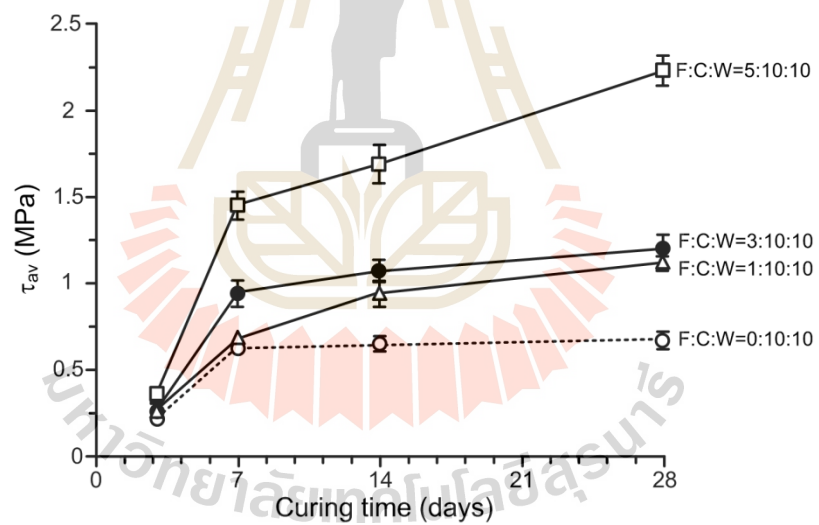


Figure 5.11 Bond strength test fly ash-mixed cement as a function of curing time.

The failure modes are recorded. The test results are presented in forms of the shear strength as a function of normal stress as follows:

$$\tau = F/A \quad (5.4)$$

where τ is the shear stress, F is sheared force, A is cross section area.

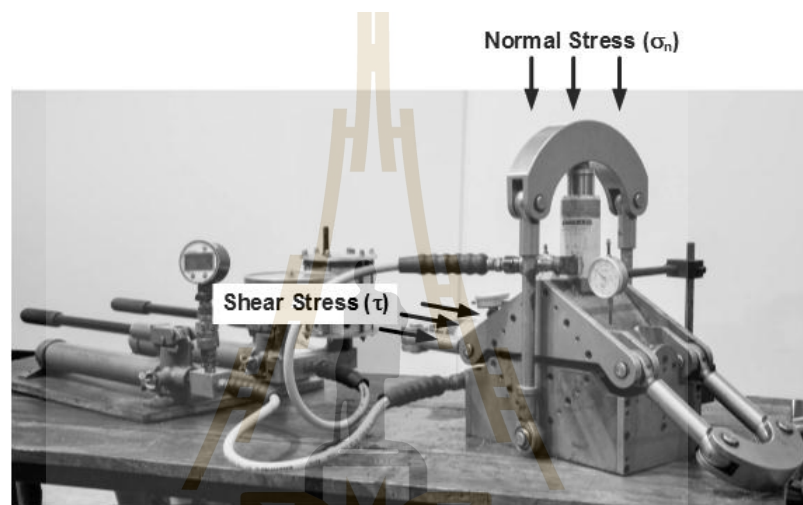


Figure 5.12 The direct shear machine model EL-77-1030 for direct shear tests.

The results are presented in the form of the Coulomb's criterion. The line tangent to each of these circles defines the Coulomb's criterion and can be expressed by:

$$\tau = c_p + \sigma \tan \phi_p \quad (5.5)$$

where τ and σ are the shear stress and normal stress, ϕ_p is the angle of internal friction, and c_p is cohesion.

Figure 5.13 shows some samples before testing. Table 5.5 lists the result of shear strength. Shearing resistance between cement grout and fracture are shown in Figures 5.14 to 5.17. Table 5.6 lists the Coulomb's parameters. The results in the form of the Coulomb's criterion are shown in Figure 5.18.

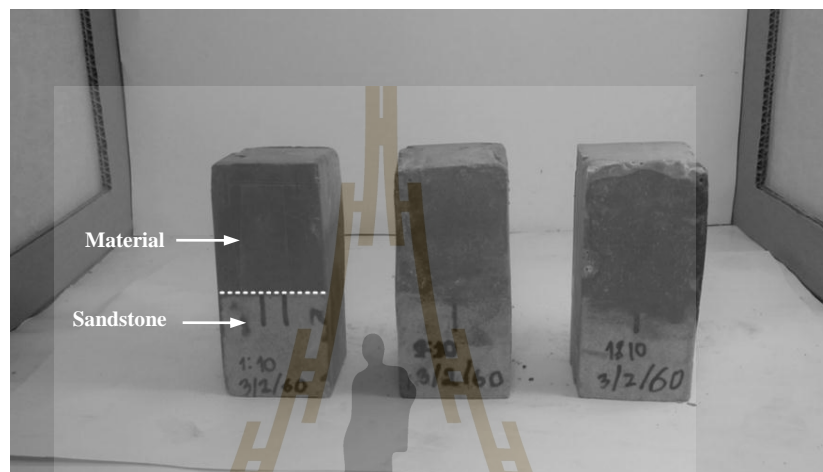


Figure 5.13 Some specimens of $54.0 \times 54.0 \times 108.0 \text{ mm}^3$ prepared for direct shear testing.

Table 5.8 Summary of Direct shear strength test results on the F:C:W, and B:C:W mixtures specimens.

Normal Stress (MPa)	Peak Shear Stress (MPa)						
	F:C:W				B:C:W (Wetchasat, 2013)		
	0:10:10	1:10:10	3:10:10	5:10:10	1:10:10	2:10:10	3:10:10
0.25	0.89	0.93	1.11	1.44	0.37	0.22	0.25
0.75	1.06	1.13	1.41	2.06	0.65	0.43	0.47
1.25	1.30	1.44	2.23	3.05	0.85	0.63	0.67

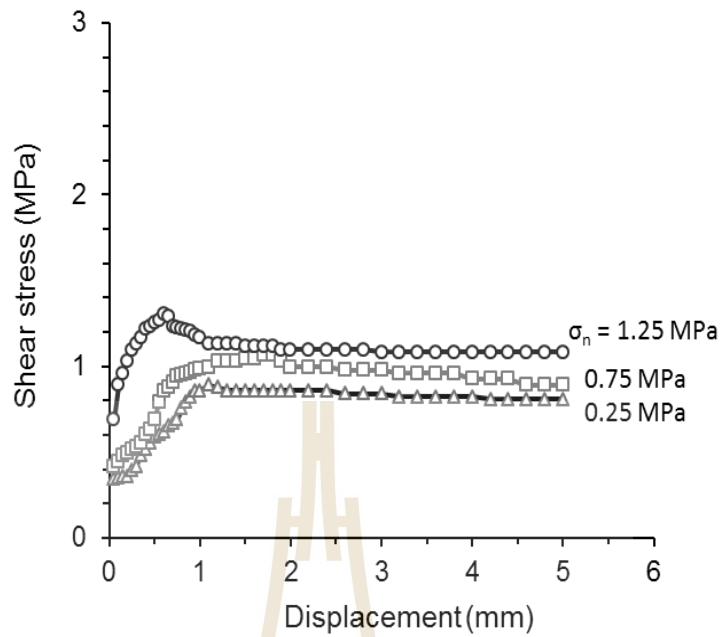


Figure 5.14 Shear stress as a function of shear displacement for pure cement.

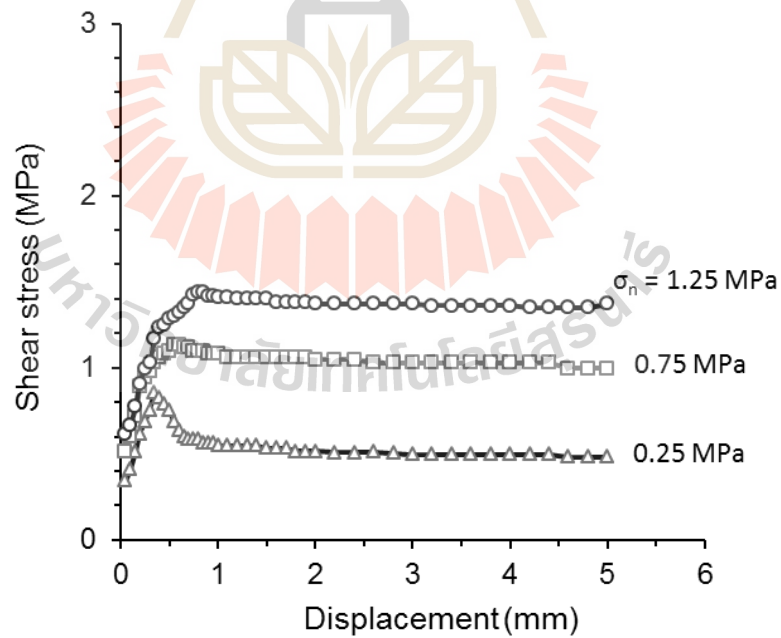


Figure 5.15 Shear stress as a function of shear displacement for F:C:W=1:10:10.

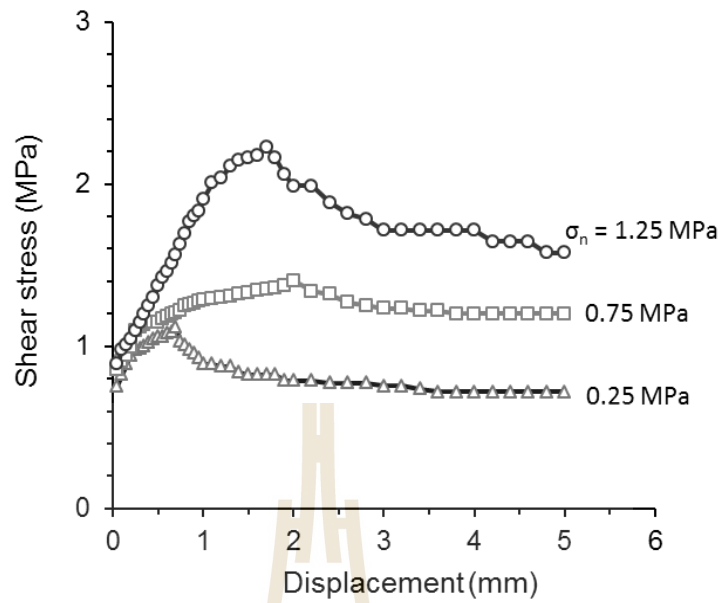


Figure 5.16 Shear stress as a function of shear displacement for F:C:W=3:10:10.

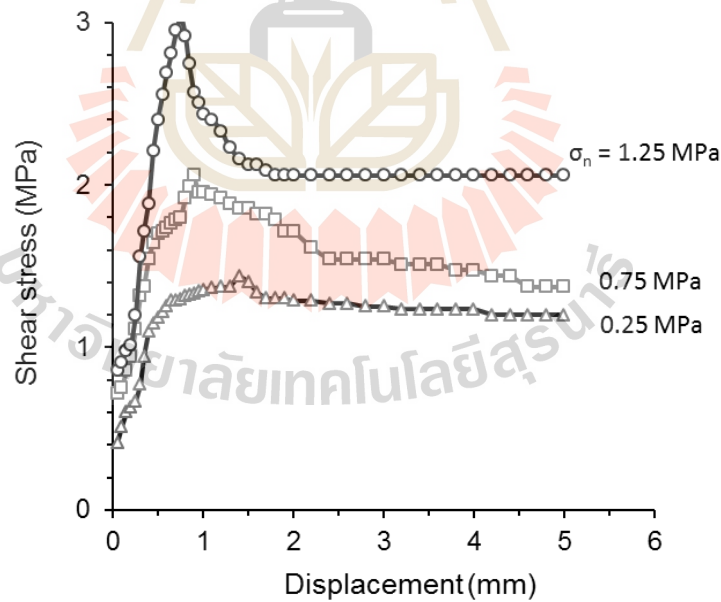


Figure 5.17 Shear stress as a function of shear displacement for F:C:W=5:10:10.

Table 5.9 Summary of shear strength parameters calibrated from direct shear tests using Coulomb's criteria.

Sample No.	Ratio	c_p (MPa)	ϕ_p (degrees)	$\tan\phi_p$	R^2
F:C:W	0:10:10	0.78	22.30	0.41	0.99
	1:10:10	0.78	27.00	0.51	0.99
	3:10:10	0.74	48.20	1.12	0.93
	5:10:10	0.98	58.20	1.61	0.98
B:C:W (Wetchasat, 2013)	1:10:10	0.31	23.00	0.42	0.97
	2:10:10	0.12	22.30	0.41	0.99
	3:10:10	0.14	23.30	0.43	0.99

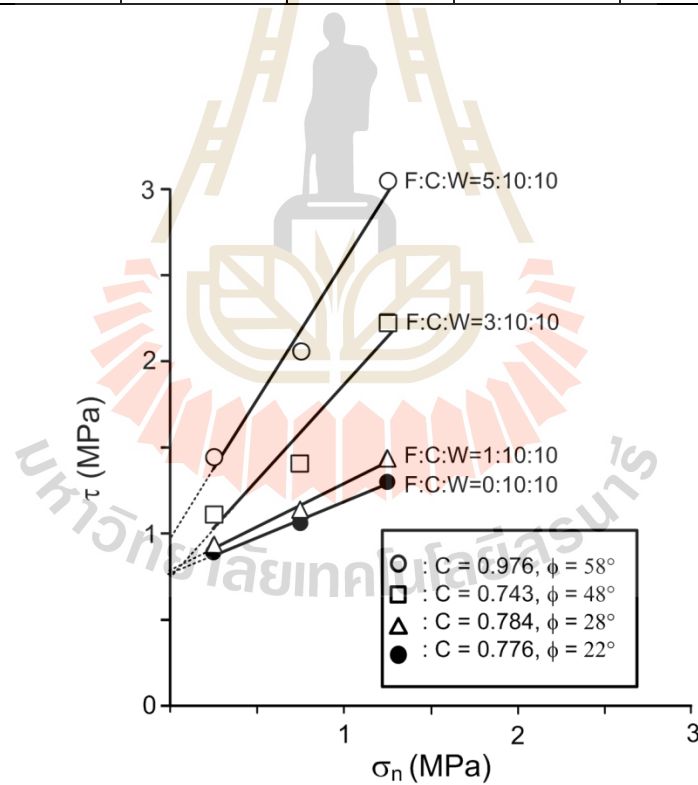


Figure 5.18 Shear stress as a function of normal stress.

CHAPTER VI

HYDRAULIC PROPERTIES TESTING

6.1 Introduction

This chapter describes the methods and results of laboratory tests to determine the permeability of grouting materials in artificial fractures from Phu Kradung sandstone. The permeability of the mixture is an important factor to show the hydraulic potential, otherwise the ability to reduce permeability of fractures in sandstone. Hydraulic properties testing in this chapter are divided into three tasks: 1) grout permeability tests, 2) fracture permeability tests, and 3) permeability test of grouting materials in rock fractures. The rock samples are prepared as described in Chapter III.

6.2 Permeability of grouting materials

The objective of the grout permeability tests is to determine the water permeability of grouting material specimen using constant head flow tests. The permeability of grouting material is the factor to be used to determine the most suitable mixing ratios for grouting in rock. These tasks describe a method for grout permeability testing in the laboratory. Proportions of F:C:W mixtures are 1:10:10, 3:10:10, and 5:10:10 by weight. The procedure for determining the grout permeability is similar to the ASTM C938 and C39. These tests are conducted at 3, 7, 14, 28, and 60 days of curing.

The mold has an inner diameter of 98.0 mm with a length of 125.0 mm. The prepared specimen is sealed between two acrylic plates with the aid of O-ring rubber and epoxy coating (Figures 6.1 and 6.2). Inlet ports are installed at the end of the mold and connected to a water pressure tube. Nitrogen compressed with pressure up to 68.9 kPa. Air bubbles are bled out before measuring the permeability. Outlet ports are installed at another end and connected to a high precision pipette for measuring the outflow (Figures 6.3 and 6.4). The intrinsic permeability (k) is calculated from the flow rate based on Darcy's law (Freeze and Cherry, 1979; Indraratna and Ranjith 2001).

Table 6.1 summarizes the results of permeability testing of grouting material results at 3, 7, 14, 28, and 60 days of curing. The results of comparison of F:C:W mixtures and B:C:W mixtures are presented on Figure 6.5.

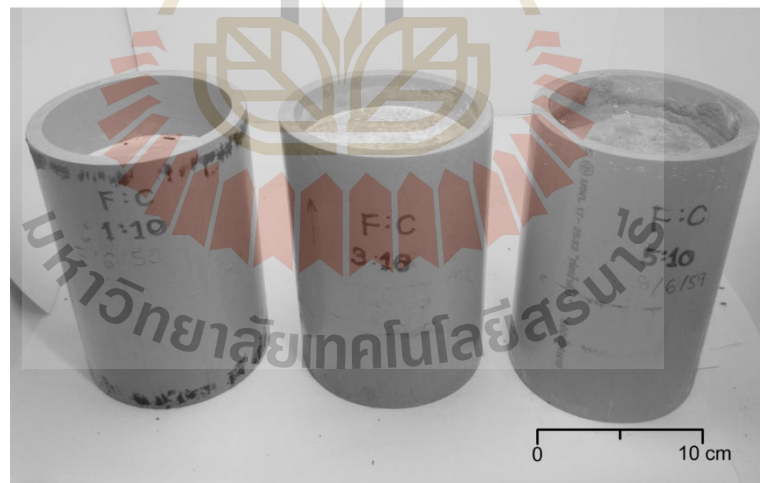


Figure 6.1 PVC mold has an inside diameter of 101.6 mm for permeability testing of grouting materials.



Figure 6.2 PVC mold has sealed between two acrylic platens with the aid of O-ring rubber and epoxy coating for permeability testing of grouting materials.

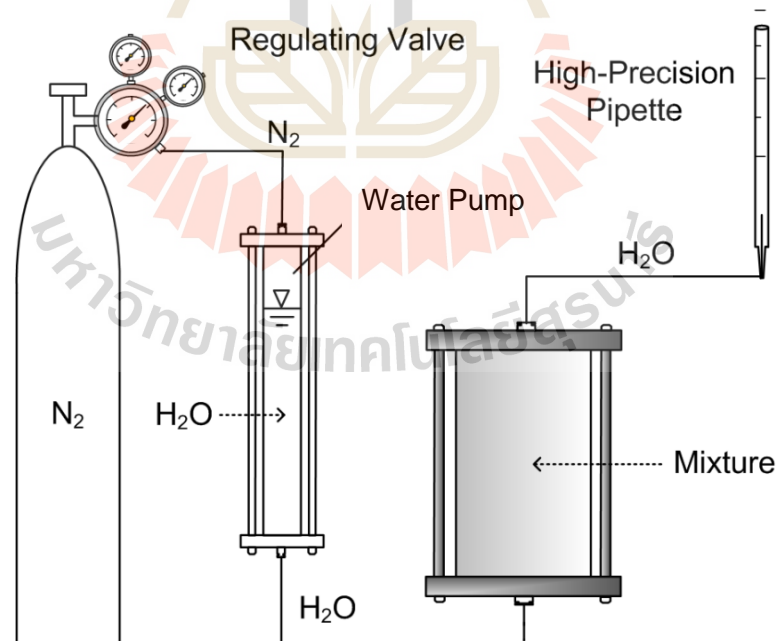


Figure 6.3 Diagram of laboratory arrangement for permeability testing of grouting materials.

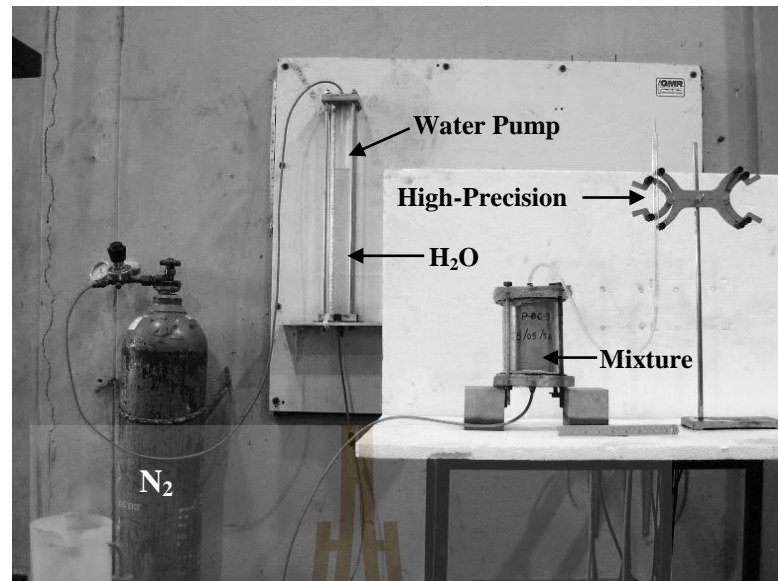


Figure 6.4 Laboratory arrangements for permeability testing of grouting materials.

Table 6.1 Summary of permeability testing of grouting material results at 3, 7, 14, 28, and 60 days of curing times.

Curing Time (days)	Intrinsic Permeability ($\times 10^{-18} \text{ m}^2$)						
	F:C:W				B:C:W (Wetchasat, 2013)		
	1:10:10	3:10:10	5:10:10	0:10:10	1:10:10	2:10:10	3:10:10
3	12196.7	5272.9	2046.6	8930.0	2,370.0	868.0	317.0
7	6305.4	2608.0	1653.0	965.0	431.0	265.0	67.6
14	3687.0	2090.9	1225.9	74.1	414.0	228.0	49.0
28	2311.0	997.9	754.7	0.441	356.0	208.0	41.3
60	329.3	154.2	100.6	-	-	-	-

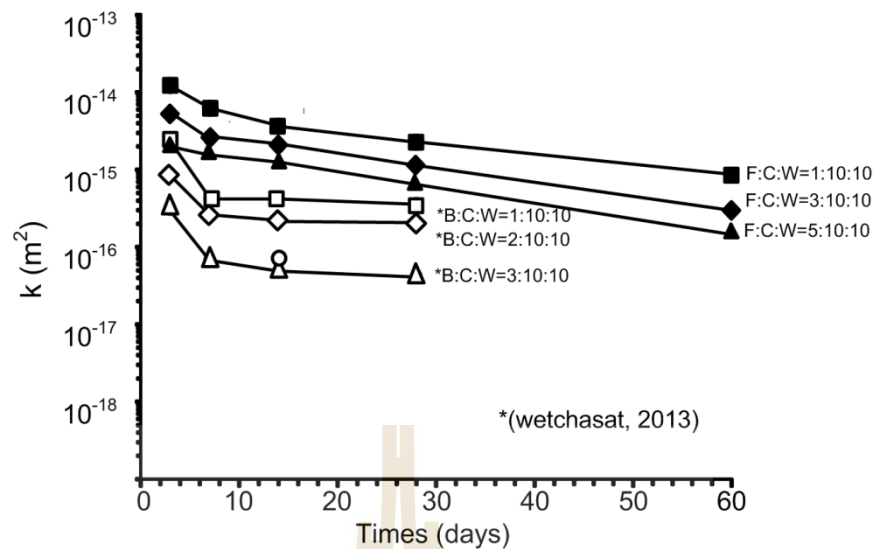


Figure 6.5 Intrinsic permeability as a function of time for B:C:W, and F:C:W ratio.

6.3 Permeability of rock fractures

The objective of this task is to assess the permeability of rock fractures under varying normal stresses. The fracture permeability is used to compare with the permeability of grouting materials for both fly ash and bentonite mixtures. The normal stresses are different. The rock samples in $130.0 \times 130.0 \times 130.0 \text{ mm}^3$ prismatic blocks are prepared as described in Chapter III (Figures 6.6 and 6.7).

The constant head flow tests are performed. The normal stresses are ranging from 1, 2, 3 and 4 MPa. Three specimens are prepared and tested. The injection hole at the center of the upper block is 10 mm in diameter and 130.0 mm in depth. The tests are conducted by injecting water. Injecting water conducted the tests into the center hole of the rectangular block specimen. The laboratory arrangement of the constant head flow test is shown in Figure 6.8. Water volume and time are recorded that tend to decrease exponentially with the normal stress. The equivalent hydraulic aperture (e_h) for radial flow, hydraulic conductivity between smooth and parallel

plates (K), and intrinsic permeability (k) are calculated by (Tsang, 1992; Indraratna and Ranjith, 2001):

$$e_h = \{[(6\mu q)/(\pi\Delta P)] \ln(r/r_0)\}^{1/3} \quad (6.1)$$

$$K = \gamma_w e_h^2/12\mu \quad (6.2)$$

$$k = e_h^2/12 \quad (6.3)$$

where μ is the dynamic viscosity of the water ($\text{N}\cdot\text{s}/\text{cm}^2$), q is water flow rate through the specimen (cm^3/s), ΔP is injecting water pressure into the center hole of rectangular blocks of the specimen, r is radius of flow path (m), r_0 is radius of the radius injection hole (m). γ_w is unit weight of water (N/m^2).



Figure 6.6 Some sandstone specimens of $130 \times 130 \times 130 \text{ mm}^3$ prepared for permeability testing of rock fractures.

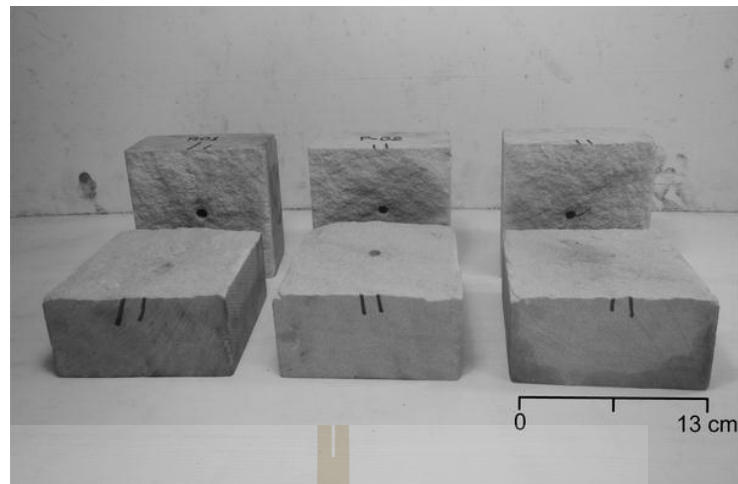


Figure 6.7 Fracture surface in sandstone specimen prepared for permeability testing of rock fractures.



Figure 6.8 Laboratory arrangements for permeability testing of fractures

Table 6.2 Summary of permeability of rock fractures results.

Sample No.	Normal stress (MPa)	e_h (μm)	K (10^{-3} m/s)	k (10^{-9} m ²)
1	1	32.217±2.63	0.838±0.01	0.087±0.08
	2	27.613±3.49	0.616±0.02	0.064±0.04
	3	24.428±2.76	0.482±0.00	0.050±0.12
	4	23.646±2.25	0.452±0.01	0.047±0.03
2	1	31.609±3.49	0.807±0.00	0.083±0.05
	2	29.564±4.38	0.706±0.01	0.073±0.06
	3	28.331±1.23	0.648±0.02	0.067±0.11
	4	27.963±2.29	0.632±0.01	0.065±0.23
3	1	19.306±3.35	0.301±0.03	0.031±0.08
	2	15.626±0.85	0.197±0.02	0.020±0.09
	3	15.323±3.23	0.190±0.04	0.020±0.05
	4	13.849±4.60	0.155±0.04	0.016±0.17

Table 6.2 lists the result of permeability of rock fractures under normal stresses ranging from 1, 2, 3 and 4 MPa. Figure 6.9 is shown relationship of intrinsic permeability (k), hydraulic conductivity (K), and aperture (e_h) as a function of normal stress (σ_n) for fracture in Phu Kradung sandstone.

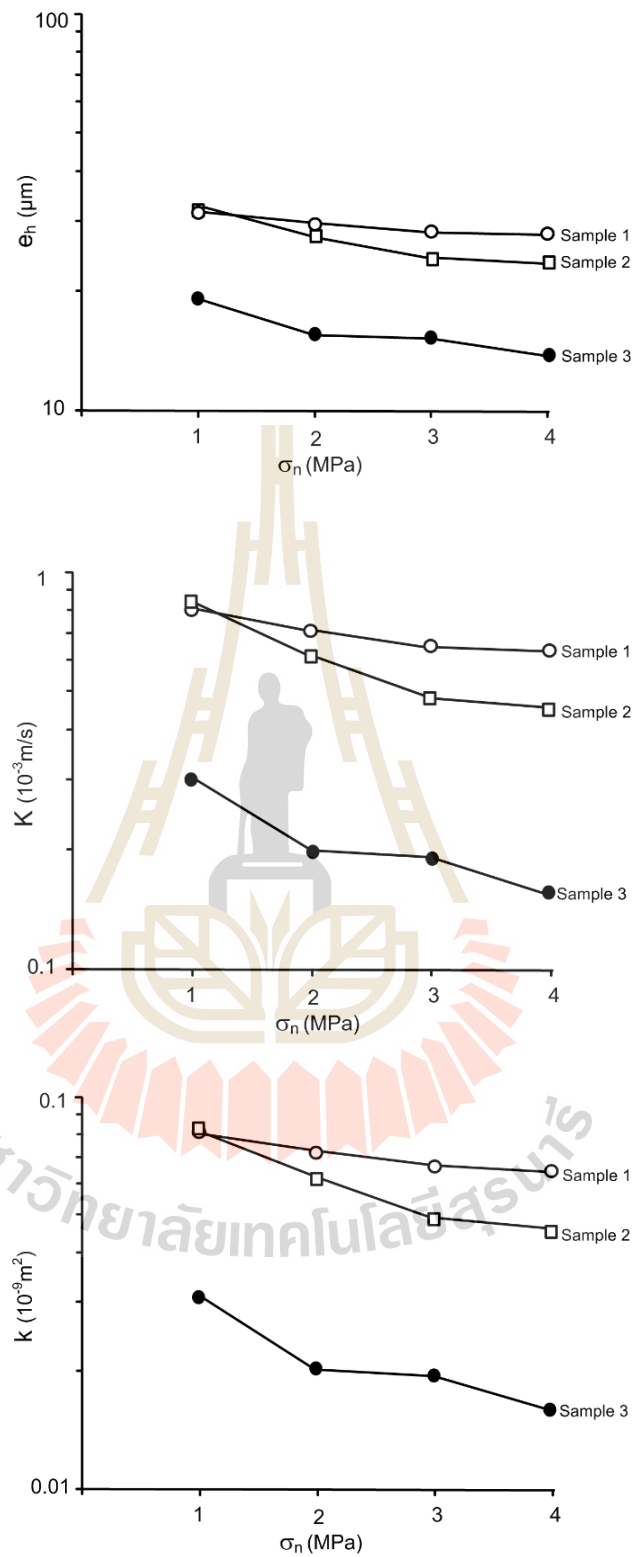


Figure 6.9 Intrinsic permeability (k), hydraulic conductivity (K), and aperture (e_n) as a function of normal stress (σ_n) for fracture in Phu Kradung sandstone.

6.4 Permeability of grouting materials in rock fractures

The objective of permeability test of grouting materials in rock fractures is to determine the permeability of fly ash-mixed cement and bentonite-mixed cement in artificial fractures from Phu Kradung sandstone. Three mixture proportions of F:C:W and prepared are similar Chapter IV. The grouting materials are used to fill the fractures.

The testing method is similar to that described above this task. The grouting materials are injected into the fractures. The fracture apertures are 2, 10, and 20 mm Figures 6.10. The grouting materials are cured for 7 days. Figures 6.11 to 6.12 give the laboratory arrangement. Constant head flow tests is performed. The constant head is ranging between 13.8 and 551.7 kPa.

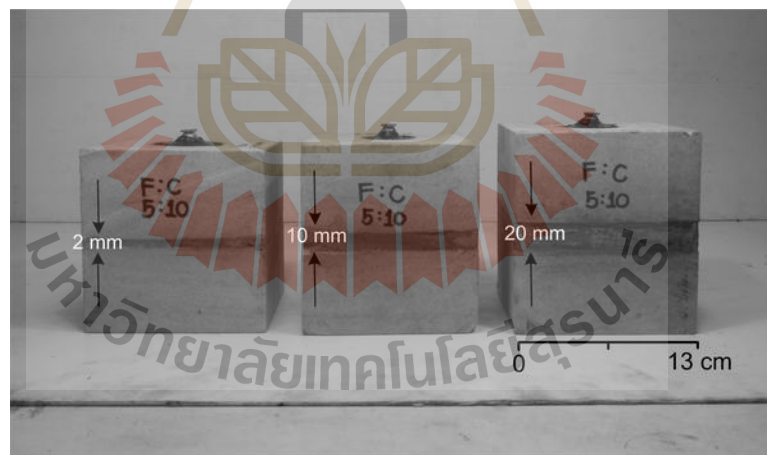


Figure 6.10 Some sandstone specimens prepared for permeability testing of grouting materials in rock fractures at fracture aperture 2, 10, and 20 mm.

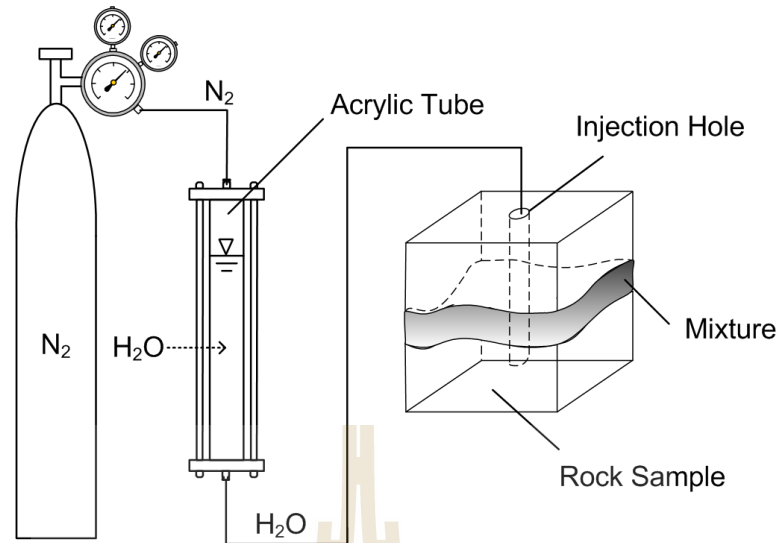


Figure 6.11 Diagram of laboratory arrangement for permeability testing of grouting materials in rock fracture.

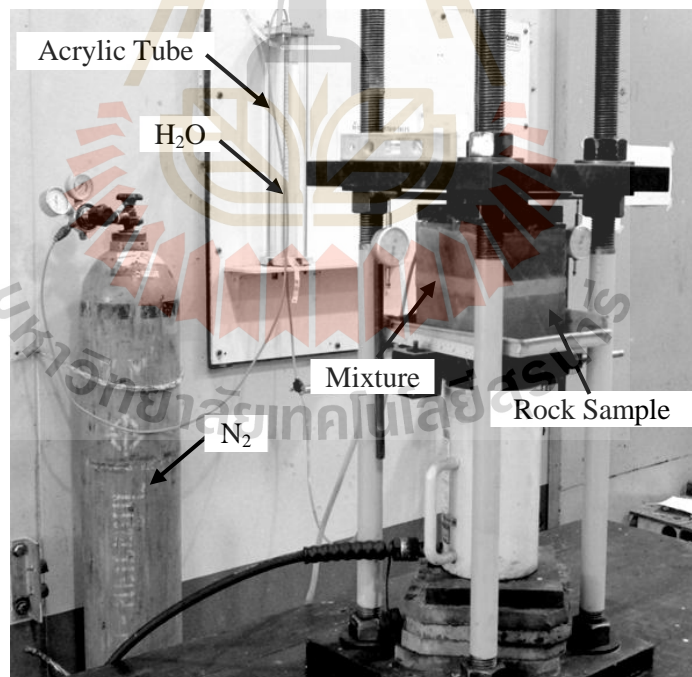


Figure 6.12 Permeability testing of grouting materials in rock fracture.

The constant normal stresses are 0.25, 0.5, 0.75, 1.0 and 1.25 MPa. The results show that the normal stress can reduce the permeability of grouting materials in fractured sandstone. The intrinsic permeability (k) is calculated from the measured flow rate (Q) as follows: (Indraratna and Ranjith, 2001):

$$K = \frac{Q \ln(2mL/D)}{2\pi L H_c} \quad (6.4)$$

$$k = \frac{K\mu}{\gamma_w} \quad (6.5)$$

where K is hydraulic conductivity, Q is flow rate of water flow through the mixture, m is square root of the ratio between the conductivity perpendicular and parallel to the hole (here, m is equal to 1), L is the thickness of grouting material in fracture apertures, D is diameter of the injection hole at the center of the upper block, H_c is the constant head used for the test, μ is dynamic viscosity (891×10^{-6} kg/ m·s) at temperature of 25°C, γ_w is unit weight of water (997.13 kg/m³).

The results of permeability of grouting material in rock fractures aperture 2, 10, and 20 mm are summarized in Tables 6.3 - 6.5. Intrinsic permeability (k), hydraulic conductivity (K), and aperture (e_h) as a function of normal stress (σ_n) for fracture aperture 2, 10, and 20 mm are shown in Figures 6.13 - 6.15.

Table 6.3 Summary of permeability of grouting material in rock fractures aperture 2 mm.

Binder	Normal stress (MPa)	e_h (μm)	K (10^{-9} m/s)	k (10^{-15} m²)
F:C:W = 0:10:10	0.25	0.77±0.01	484.73±1.60	50.01±0.70
	0.50	0.74±0.00	447.23±2.28	46.14±0.61
	0.75	0.74±0.01	436.82±2.70	45.07±0.76
	1.00	0.71±0.02	401.79±2.27	41.46±0.39
	1.25	0.69±0.01	379.46±1.74	39.15±1.52
F:C:W = 1:10:10	0.25	0.72±0.01	422.10±2.05	43.55±0.32
	0.50	0.71±0.00	401.79±0.15	41.46±0.39
	0.75	0.67±0.10	362.97±1.44	37.45±0.39
	1.00	0.67±0.00	361.22±0.86	37.27±0.19
	1.25	0.67±0.01	359.49±3.18	37.09±0.77
F:C:W = 3:10:10	0.25	0.53±0.01	227.68±0.23	23.49±1.07
	0.50	0.44±0.01	155.88±2.04	16.08±0.65
	0.75	0.39±0.01	123.58±3.13	12.75±1.59
	1.00	0.37±0.01	111.31±0.93	11.48±0.36
	1.25	0.33±0.01	87.88±0.48	9.07±0.75
F:C:W = 5:10:10	0.25	2.84±0.28	6533.38±5.93	674.09±2.05
	0.50	2.45±0.21	4847.35±3.07	500.13±7.68
	0.75	2.31±0.14	4293.36±3.99	442.98±0.72
	1.00	2.27±0.17	4174.10±2.05	430.67±1.89
	1.25	1.84±0.06	2732.14±3.64	281.89±2.20

Table 6.3 Summary of permeability of grouting material in rock fractures aperture 2 mm
(continued), (Wetchasat, 2013).

Binder	Normal stress (MPa)	e_h (μm)	K (10^{-9} m/s)	k (10^{-15} m²)
B:C:W = 1:10:10	0.25	4.95±0.30	191.03±23.65	17.07±2.11
	0.50	4.08±0.12	129.69±7.87	11.59±0.70
	0.75	3.36±0.31	88.27±15.57	7.89±1.39
	1.00	2.84±0.10	62.70±4.33	5.60±0.39
	1.25	2.37±0.29	44.08±10.42	3.94±0.93
B:C:W = 2:10:10	0.25	5.96±0.41	277.04±38.01	24.75±3.40
	0.50	4.95±0.36	191.30±26.97	17.09±2.41
	0.75	4.05±0.24	128.01±15.11	11.44±1.35
	1.00	3.27±0.19	83.42±9.32	7.45±0.83
	1.25	2.58±0.10	51.78±3.82	4.63±0.34
B:C:W= 3:10:10	0.25	4.27±0.16	141.51±10.42	12.65±0.93
	0.50	3.64±0.20	103.12±11.08	9.21±0.99
	0.75	3.05±0.20	72.68±9.42	6.49±0.84
	1.00	2.60±0.12	52.59±4.72	4.70±0.42
	1.25	2.17±0.06	36.70±2.06	3.28±0.18

Table 6.4 Summary of permeability of grouting material in rock fractures aperture 10 mm.

Binder	Normal stress (MPa)	e_h (μm)	K (10^{-9} m/s)	k (10^{-15} m²)
F:C:W = 0:10:10	0.25	0.80±0.01	512.54±1.80	52.88±1.50
	0.50	0.78±0.00	486.03±1.39	50.15±1.31
	0.75	0.74±0.01	447.46±2.44	46.17±0.83
	1.00	0.72±0.02	420.74±1.60	43.41±2.41
	1.25	0.67±0.02	366.10±2.90	37.77±0.51
F:C:W = 1:10:10	0.25	0.44±0.02	153.21±1.27	15.81±0.14
	0.50	0.37±0.01	110.55±0.32	11.41±0.42
	0.75	0.32±0.02	85.17±0.59	8.79±0.15
	1.00	0.27±0.01	58.61±2.55	6.05±0.74
	1.25	0.24±0.01	54.74±1.58	5.65±0.81
F:C:W = 3:10:10	0.25	0.34±0.01	91.82±0.83	9.47±0.37
	0.50	0.26±0.02	52.99±1.42	5.47±0.38
	0.75	0.23±0.02	41.33±2.59	4.26±0.17
	1.00	0.21±0.01	34.59±1.83	3.57±0.26
	1.25	0.18±0.00	27.64±0.26	2.85±0.46
F:C:W = 5:10:10	0.25	1.21±0.18	1174.57±1.72	121.19±0.57
	0.50	1.17±0.24	1105.48±3.90	114.06±2.79
	0.75	1.13±0.21	1025.08±3.59	105.76±2.66
	1.00	1.11±0.21	989.11±1.50	102.05±1.45
	1.25	1.09±0.21	955.59±6.07	98.59±4.31

Table 6.4 Summary of permeability of grouting material in rock fractures aperture 10 mm

(continued), (Wetchasat, 2013).

Binder	Normal stress (MPa)	e_h (μm)	K (10^{-9} m/s)	k (10^{-15} m²)
B:C:W = 1:10:10	0.25	0.52±0.01	2.12±0.10	0.19±0.01
	0.50	0.43±0.01	1.46±0.04	0.13±0.00
	0.75	0.36±0.01	1.01±0.04	0.09±0.00
	1.00	0.30±0.00	0.69±0.02	0.06±0.00
	1.25	0.25±0.00	0.48±0.01	0.04±0.00
B:C:W = 2:10:10	0.25	1.12±0.02	9.78±0.27	0.87±0.02
	0.50	0.90±0.03	6.34±0.45	0.57±0.04
	0.75	0.74±0.03	4.31±0.34	0.38±0.03
	1.00	0.61±0.01	2.90±0.14	0.26±0.01
	1.25	0.52±0.01	2.10±0.06	0.19±0.00
B:C:W = 3:10:10	0.25	1.56±0.03	18.93±0.84	1.69±0.08
	0.50	1.28±0.03	12.69±0.59	1.13±0.05
	0.75	1.05±0.01	8.60±0.14	0.77±0.01
	1.00	0.87±0.04	5.88±0.57	0.53±0.05
	1.25	0.71±0.02	3.91±0.25	0.35±0.02

Table 6.5 Summary of permeability of grouting material in rock fractures aperture 20 mm.

Binder	Normal stress (MPa)	e_h (μm)	K (10^{-9} m/s)	k (10^{-15} m²)
F:C:W = 0:10:10	0.25	0.91±0.01	668.60±1.84	68.98±1.43
	0.50	0.85±0.00	615.82±2.90	63.54±1.03
	0.75	0.83±0.01	570.76±3.00	54.89±0.08
	1.00	0.75±0.01	405.72±2.23	50.35±0.09
	1.25	0.72±0.01	377.57±3.94	46.43±1.22
F:C:W = 1:10:10	0.25	0.58±0.01	272.11±0.07	28.08±0.65
	0.50	0.50±0.01	205.27±0.90	21.18±0.58
	0.75	0.46±0.01	168.35±1.66	17.37±0.09
	1.00	0.45±0.01	164.80±1.27	17.00±0.71
	1.25	0.43±0.00	148.11±2.20	15.28±0.20
F:C:W = 3:10:10	0.25	0.26±0.00	53.18±1.28	5.49±0.11
	0.50	0.24±0.00	45.18±1.29	4.66±0.10
	0.75	0.22±0.00	38.24±2.29	3.95±0.07
	1.00	0.22±0.01	37.74±1.23	3.89±0.10
	1.25	0.20±0.01	32.23±0.54	3.33±0.08
F:C:W = 5:10:10	0.25	1.31±0.20	1376.53±1.08	142.03±4.22
	0.50	0.91±0.23	778.60±1.84	95.78±2.82
	0.75	0.87±0.20	655.30±7.63	68.98±0.81
	1.00	0.81±0.23	458.84±9.79	56.15±2.72
	1.25	0.75±0.17	398.8±5.67	49.27±0.66

Table 6.5 Summary of permeability of grouting material in rock fractures aperture 20 mm
(continued), (Wetchasat, 2013).

Binder	Normal stress (MPa)	e_h (μm)	K (10^{-9} m/s)	k (10^{-15} m ²)
B:C:W = 1:10:10	0.25	1.10±0.07	9.42±1.18	0.84±0.11
	0.50	0.94±0.04	6.95±0.60	0.62±0.05
	0.75	0.83±0.04	5.33±0.51	0.48±0.05
	1.00	0.72±0.03	4.04±0.38	0.36±0.03
	1.25	0.64±0.04	3.24±0.38	0.29±0.03
B:C:W = 2:10:10	0.25	3.06±0.25	73.26±11.81	6.55±1.06
	0.50	2.34±0.22	42.97±8.21	3.84±0.73
	0.75	1.90±0.28	28.37±8.14	2.54±0.73
	1.00	1.51±0.11	17.73±2.51	1.58±0.22
	1.25	1.26±0.03	12.34±0.55	1.10±0.05
B:C:W= 3:10:10	0.25	0.95±0.04	7.05±0.60	0.63±0.05
	0.50	0.80±0.03	4.94±0.31	0.44±0.03
	0.75	0.70±0.05	3.85±0.58	0.34±0.05
	1.00	0.63±0.05	3.10±0.48	0.28±0.04
	1.25	0.56±0.03	2.43±0.23	0.22±0.02

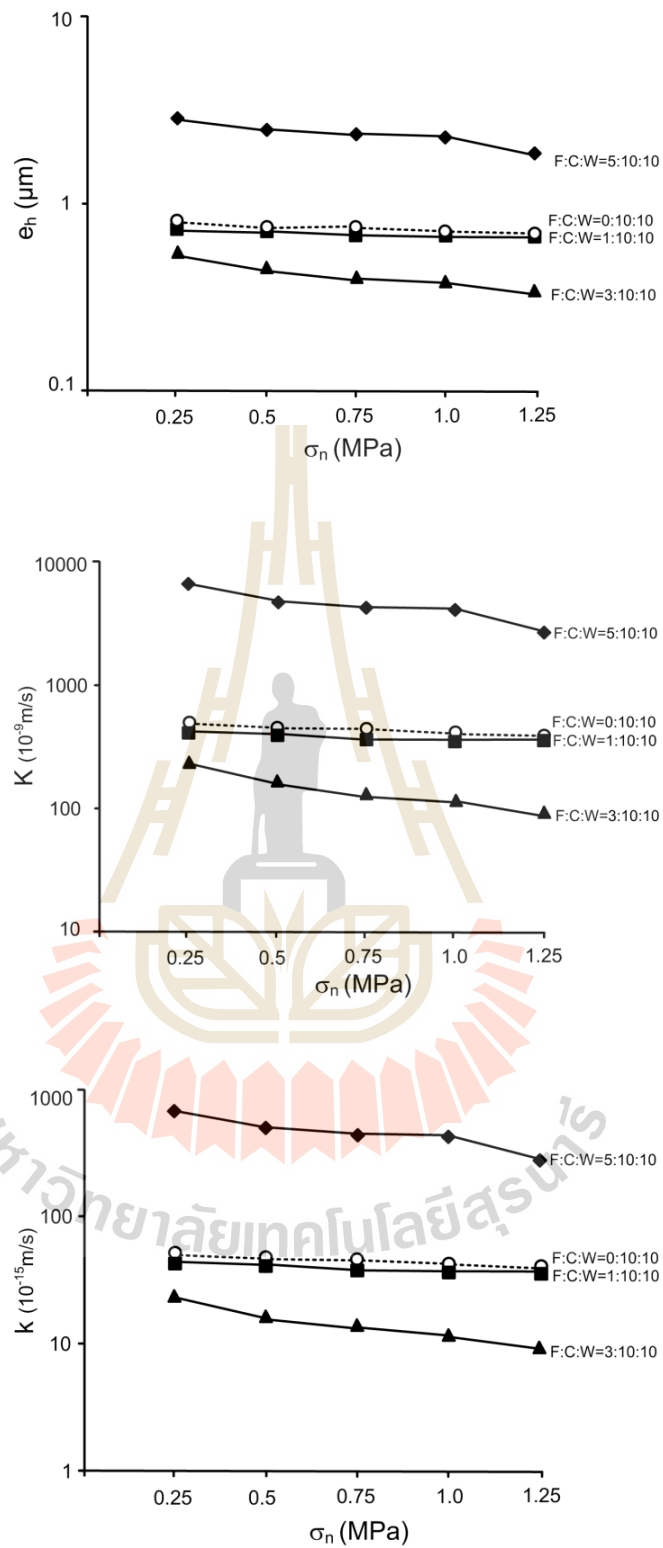


Figure 6.13 Intrinsic permeability (k), hydraulic conductivity (K), and aperture (e_h) as a function of normal stress (σ_n) for fracture aperture 2 mm.

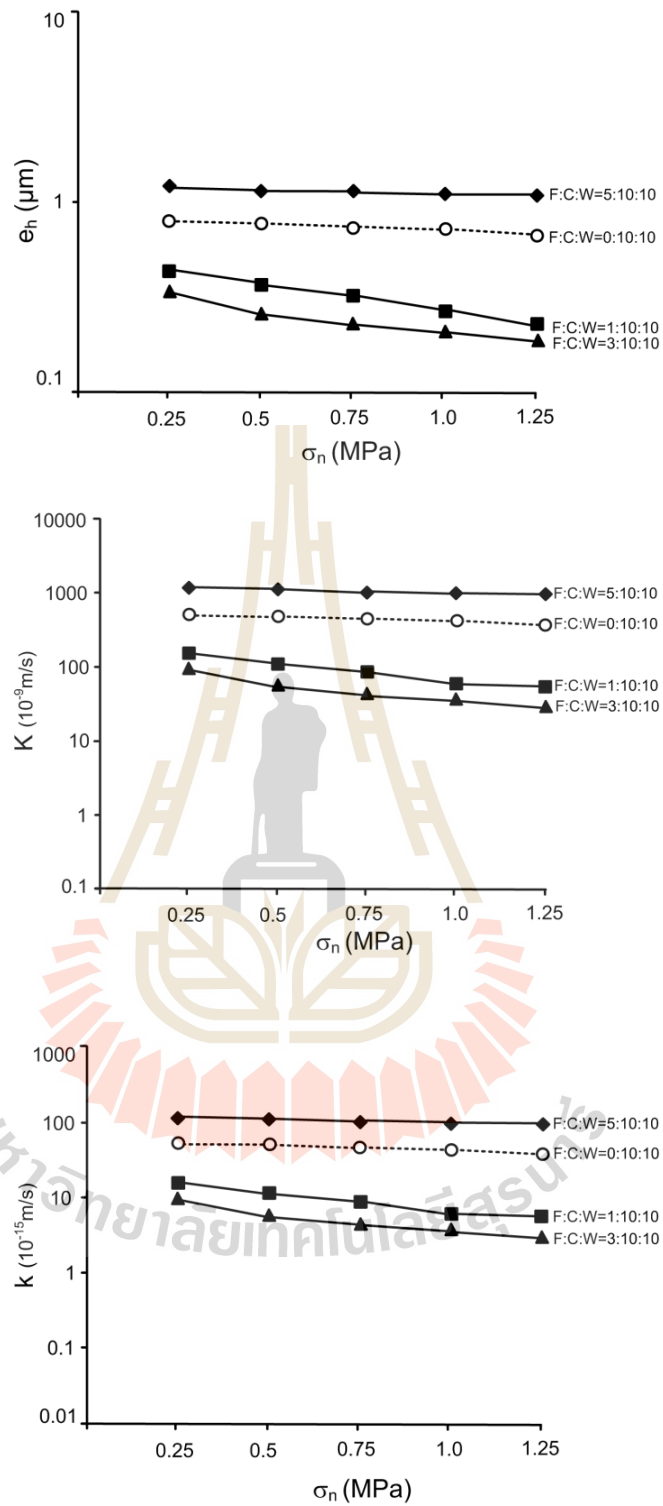


Figure 6.14 Intrinsic permeability (k), hydraulic conductivity (K), and aperture (e_h) as a function of normal stress (σ_n) for fracture aperture 10 mm.

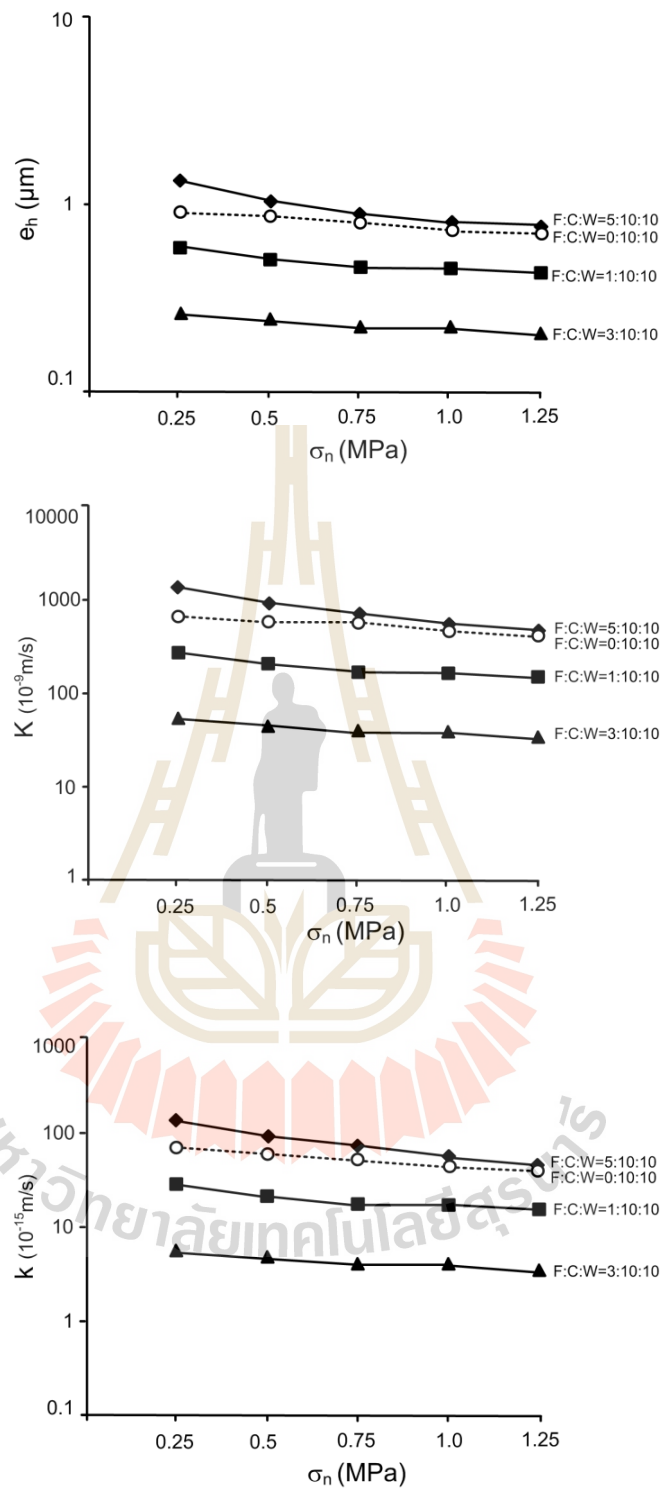


Figure 6.15 Intrinsic permeability (k), hydraulic conductivity (K), and aperture (e_h) as a function of normal stress (σ_n) for fracture aperture 20 mm.

CHAPTER VII

DISCUSSIONS, CONCLUSIONS AND RECOMMENDATION FOR FUTURE STUDIES

7.1 Discussions and conclusions

The fly ash is classified as Class C by ASTM C618 standard. The average liquid limit, plastic limit and plasticity index are 20.71%, 16.92%, and 3.79%, respectively. It has a spherical shape with its specific gravity of 2.67, is classified as inorganic silt with over 80% of its particles smaller than 0.1 mm. This study aim to determine the minimum slurry viscosity and appropriate strength of the grouting materials. Grouting materials in the study are contained fly ash (F), cement (C), and water (W) for F:C:W mixtures and bentonite (B), cement (C) and water (W) for B:C:W mixtures. The mechanical and hydraulic tests of mixtures are determined to select the appropriate proportions of fly ash-to-cement and bentonite-to-cement ratios for grouting material in rock fractures.

The basic properties of the mixtures slurry are initially designed to select the appropriate proportions of fly ash-to-cement ratios. The fly ash-mixed cement ratios (F:C:W) of 0:10:10, 1:10:10, 3:10:10, 5:10:10, 6:10:10, 7:10:10, 8:10:10, 9:10:10, 10:10:10, 15:10:10, and 20:10:10 by weight. The bentonite-cement ratios (B:C:W) are 0:10:10, 1:10:10, 2:10:10, and 3:10:10 by weight. A mixing of all grouts is by using a blade paddle mixer as suggested by ASTM C938 (ASTM 2010a).

The mixture of proportions (F:C:W, B:C:W) that more than 5:10:10 by weight cannot be used to make the grouting material due to it is high viscosity and hence cannot flow in fractures. The proportions of mixtures are comparable to Garvin and Hayles (1999), they are the B:C proportion of 0.33. This study uses the B:C:W mixtures of 1:10:10, 2:10:10, and 3:10:10 and the F:C:W mixtures of 1:10:10, 3:10:10, and 5:10:10. The viscosity measurement follows, as much as practical, the ASTM D2196. The results are shown in Figure 4.11. The viscosity is measured with Brookfield® viscometer. The dynamics viscosity of cement slurries tends to increase as the mixed cement ratios increasing. These proportions yield the lowest slurry viscosity of about 5 Pa·s.

The uniaxial compressive strength and elastic modulus of the grouting materials are determined. All specimens are cured for 3, 7, 14, and 28 days before testing. The strength of cement slurries increase with curing times increasing. The results are shown in Figure 5.4 to 5.5. The highest compressive strength is from the fly ash-mixed cement ratio of 5:10:10 after 28 day curing times. The average compressive strength (σ_c) and elastic modulus (E) is 10.45 MPa and 1360 MPa respectively.

The brazilian tensile strength of the grouting materials are determined. All specimens are cured for 3, 7, 14, and 28 days before testing. The tensile strength of cement slurries increase with curing times increasing. The results are shown in Figure 5.8. The highest tensile strength is from the fly ash-mixed cement ratio of 5:10:10 after 28 day curing times. The average brazilian tensile strength (σ_B) is 1.91 MPa.

The bond strength of the grouting materials is determined. All specimens are cured for 3, 7, 14, and 28 days before testing. The bond strength of cement slurries increase with curing times increasing. The results are shown in Figure 5.11. The

highest bond strength is from the fly ash-mixed cement ratio of 5:10:10 after 28 day curing times. The average bond strength (σ) is 2.23 MPa.

The peak shear strength at the interface between the grout and sandstone fractures varying from 0.89 to 3.05 MPa under normal stresses ranging from 0.25, 0.75, and 1.25 MPa. The results are shown in Figure 5.18. The highest shear strength is from the fly ash-mixed cement ratio of 5:10:10. The peak shear strength (τ), cohesion(c), and friction angle (ϕ) is 3.05 MPa, 0.98 MPa, and 58 degrees respectively.

The permeability of grouting materials in terms of the intrinsic permeability (k). The constant head flow test is conducted to measure the longitudinal permeability of the grout. All specimens are cured for 3, 7, 14, 28, and 60 days before testing. The results are shown in Figure 6.5. The results indicate that when the curing times increase the intrinsic permeability of cement grout decreasing. The intrinsic permeability of all mixtures is in the range of 10^{-18} to 10^{-14} m². The mixture with the F:C:W of 5:10:10 by weight gives the lowest permeability.

Hydraulic aperture (e_h) and permeability coefficient (K) and the intrinsic permeability (k) are plotted as a function of the normal stress of fracture in Figure 6.9. Fracture permeability is decrease with the normal stresses on fracture aperture increasing. This tested concluded that sandstone surface is a close fracture with the aperture and the fracture permeability had very small value (less than the value of grouting material in this study). The close fracture does not affect the geo-structural engineering.

The intrinsic permeability of the grouts measured by radial flow test in fractures with apertures of 2, 10, and 20 mm ranges from 10^{-15} to 10^{-12} m² under the normal stresses ranging from 0.25, 0.5, 0.75, 1.0, and 1.25 MPa. The permeability for all grout mixtures decrease with increasing normal stresses. The results are shown in Figure 6.13 to 6.15.

7.2 Recommendations for future studies

The test results in terms of the mechanics and hydraulic properties confirm the conclusions of this study, the testing should be required as follows.

1. The laboratory testing should be performed using different types of fly ash such as Anthracite, Bituminous, Sub-bituminous and Lignite in other locations.
2. The mechanical and hydraulic properties of the different type fly ash should be considered.



REFERENCES

- Akgün, H. (2010). Geotechnical characterization and performance assessment of bentonite/sand mixtures for underground waste repository sealing. **Applied Clay Science**. 49: 394–399.
- Akgün, H. and Daemen, J. J. K. (1999). Design implications of analytical and laboratory studies of permanent abandonment plugs. **Canadian Geotechnical**. 36: 21–38.
- Akgün, H., Koçkar, M. K. and Aktürk, Ö. (2006). Evaluation of a compacted bentonite/sand seal for underground waste repository isolation. **Environmental Geology**. 50, 331–337.
- Akgün, H., and Daemen, J. J. K. (2000). Influence of degree of saturation on the borehole sealing performance of an expansive cement grout. **Cement and Concrete Research**. 30:281–289.
- Ali MS, Khan IA and Hossain MI (2008), Chemical Analysis of Ordinary Portland Cement of Bangladesh. **Chemical Engineering Research Bulletin**. 12: 7-10.
- ASTM C114-11b. Standard Test Methods for Chemical Analysis of Hydraulic Cement. **In Annual Book of ASTM Standards**. 04.01, American Society for Testing and Materials, Philadelphia.
- ASTM C150/C150M-09. Standard Specification for Portland Cement. **In Annual Book of ASTM Standards**. 04.01. American Society for Testing and Materials, Philadelphia.
- ASTM C192-07. Standard Practice for Making and Curing Concrete Test Specimens in the Laboratory. **In Annual Book of ASTM Standards**. 04.02, American.

- ASTM C20-00. Standard Test Methods for Apparent Porosity, Water Absorption, Apparent Specific Gravity, and Bulk Density of Burned Refractory Brick and Shapes by Boiling Water. **In Annual Book of ASTM Standards.** 15.01. American Society for Testing and Materials, Philadelphia.
- ASTM C33/C33M-11. Standard Specification for Concrete Aggregates. **In Annual Book of ASTM Standards.** 04.02. American Society for Testing and Materials, Philadelphia.
- ASTM C39/C39M-10. Standard Test Method for Compressive Strength of Cylindrical Concrete Specimens. **In Annual Book of ASTM Standards.** 04.01, American Society for Testing and Materials, Philadelphia.
- ASTM C91-05. Standard Specification for Masonry Cement. **In Annual Book of ASTM Standards.** 04.01, American Society for Testing and Materials, Philadelphia.
- ASTM C938-10. Standard Practice for Proportioning Grout Mixtures for Preplaced-Aggregate Concrete. **In Annual Book of ASTM Standards.** 04.02, American Society for Testing and Materials, Philadelphia.
- ASTM D2196-10. Standard Test Methods for Rheological Properties of Non-Newtonian Materials by Rotational (Brookfield type) Viscometer. **In Annual Book of ASTM Standards.** 06.01, American Society for Testing and Materials, Philadelphia.
- ASTM D2487-11. Standard Practice for Classification of Soils for Engineering Purposes (Unified Soil Classification System). **In Annual Book of ASTM Standards.** 04.08, American Society for Testing and Materials, Philadelphia.

- ASTM D3967-08. Standard test Method for Splitting Tensile Strength of Intact Rock Core Specimens. **In Annual Book of ASTM Standards (Vol. 04.08)**. Philadelphia: American Society for Testing and Materials.
- ASTM D422-07. Standard Test Method for Particle-Size Analysis of Soils. **Annual Book of ASTM Standards**. 04.08, American Society for Testing and Materials, Philadelphia.
- ASTM D4221-11. Standard Test Method for Dispersive Characteristics of Clay Soil by Double Hydrometer. **In Annual Book of ASTM Standards**. 04.08, American Society for Testing and Materials, Philadelphia.
- ASTM D4318-10. Standard Test Methods for Liquid Limit, Plastic Limit, and Plasticity Index of Soils. **In Annual Book of ASTM Standards**. 04.08, American Society for Testing and Materials, Philadelphia.
- ASTM D4543-08. Standard Practices for Preparing Rock Core as Cylindrical Test Specimens and Verifying Conformance to Dimensional and Shape Tolerances. **In Annual Book of ASTM Standards**. 04.01, American Society for Testing and Materials, Philadelphia.
- ASTM D4832-10. Standard Test Method for Preparation and Testing of Controlled Low Strength Material (CLSM) Test Cylinders. **In Annual Book of ASTM Standards**. 04.02, American Society for Testing and Materials, Philadelphia.
- ASTM D5607-95. Standard test method for performing laboratory direct shear strength test of rock specimens under constant normal force. **In Annual Book of ASTM Standards**. 04.08, American Society for Testing and Materials, Philadelphia.

- ASTM D7012-10. Standard Test Method for Compressive Strength and Elastic Moduli of Intact Rock Core Specimens under Varying States of Stress and Temperatures. **In Annual Book of ASTM Standards.** 04.09, American Society for Testing and Materials, Philadelphia.
- ASTM D854-10. Standard Test Methods for Specific Gravity of Soil Solids by Water Pycnometer. **In Annual Book of ASTM Standards.** 04.08, American Society for Testing and Materials, Philadelphia.
- Baik, M. H., Cho, W. J. and Hahn, P. S. (2007). Erosion of bentonite particles at the interface of a compacted bentonite and a fractured granite. **Engineering Geology.** 91: 229-239.
- Barton, N. R. (1973). Review of a new shear strength criterion for rock joints. **Engineering Geology.** 7: 287-332.
- Barton, N. and Bakhtar, K. (1983). Rock joint description and modeling of the hydrothermomechanical design of nuclear waste repositories (Contact report, submitted to canmet). **Mining Research Laboratory.** Ottawa.
- Barton, N., Bandis, S. and Bakhtar, K. (1985). Strength, Deformation and Conductivity Coupling of Rock Joints. **International Journal of Rock Mechanics and Mining Sciences and Geomechanics.** 22(3): 121-140.
- Brown, E.T. (editor) (1981). Rock Characterization testing and monitoring: ISRM Suggested methods. The Commission on Rock Testing Methods, **International Society for Rock Mechanics.** Pergamon Press, New York, 211 pp.
- Butron, C., Axelsson, M. and Gustafson, G. (2009). Silica sol for rock grouting: laboratory testing of strength, fracture behavior and hydraulic conductivity. **Tunnelling and Underground Space Technology.** 24: 603-607.

- Butron, C., Gustafson, G., Fransson, A. and Funehag, J. (2010). Drip sealing of tunnels in hard rock: A new concept for the design and evaluation of permeation grouting. **Tunnelling and Underground Space Technology**. 25: 114-121.
- Castelbaum, D. and Shackelford, C. D. (2009). Hydraulic Conductivity of Bentonite Slurry Mixed Sands. **Geotechnical and Geoenvironmental Engineering**. 135(12): 1941-1956.
- Cheerarat, R. and Jaturapitakkul, C. (2004). **A Study of Disposed Fly Ash from Landfill to Replace Portland cement**. Waste Management, Vol. 24 (7), 2004, pp. 701-709.
- Daemen, J.J.K., Ran, C. (1996). Bentonite as a Waste Isolation Pilot Plant Shaft Sealing Material. **Contractor Report SAND96-1968**. Sandia National Laboratories, Albuquerque, NM.
- Detoumay, E. (1980). Hydraulic Conductivity of Closed Rock Fractures: An Experimental and Analytical Study. In **Proceeding of the 13th Canadian Rock Mechanics Symposium**. (pp 168-173). Toronto: (n.p.).
- Fransson, A. (2001). Characterisation of a fractured rock mass for a grouting field test. **Tunnelling and Underground Space Technology**. 16: 331-339.
- Fransson, A., Tsang, C. F., Rutqvist, J. and Gustafson, G. (2007a). A new parameter to assess hydromechanical effects in single-hole hydraulic testing and grouting. **International Journal of Rock Mechanics and Mining Sciences**. 44:1011-1021.
- Fransson, A., Tsang, C. F., Rutqvist, J., and Gustafson, G. (2007b). Effects of the injection grout Silica sol on bentonite. **International Journal of Rock Mechanics and Mining Sciences**. 47: 887-893.

- Freeze, R. A., and Cherry, J. A. (1979). **Groundwater**. Prentice Hall, Inc. Upper Saddle River, USA, 604p.
- Fuenkajorn, K. (2007). Design process for sealing of boreholes in rock mass. **In Proceedings of the First Thailand Symposium on Rock Mechanics**. September, 13-14, Khao Yai, Thailand, Published by Geomechanics Research Unit, Suranaree University of Technology, Nakhon Ratchasima, Thailand, pp. 245-252.
- Fuenkajorn, K. and Daemen, J.J.K. (1996). **Sealing of Boreholes and Underground Excavations in Rock**. Chapman and Hall, London.
- Gangi, A. F. (1978). Variation of Whole and Fractured Porous Rocks Permeability with Confining Pressure. **International Journal of Rock Mechanics and Mining Sciences and Geomechanics**. 15: 249-257.
- Garvin, S. L. and Hayles, C. S. (1999). The chemical compatibility of cement-bentonite cut-off wall material. **Construction and Building Materials**. 13: 329-341.
- Gleason, M. H., Daniel, D. E. and Eykhole, G. R. (1997). Calcium and sodium bentonite for hydraulic containment applications. **Journal of Geotechnical and Geoenvironmental Engineering**. pp. 438-445.
- Gothall, R., and Stille, H. (2010). Fracture – fracture interaction during grouting. **Tunnelling and Underground space Technology**. 25: 199-204.
- Greer, W. B. and Crouthamel, D. R. (1996). In-situ Hydraulic Performance of Cement Borehole Seals. **Sealing of Boreholes and Underground Excavations in Rock**. pp. 157-183. Chapman&Hall.

- Hadsanan, P., Lertpocasombut, K. and Chatveera, B. (2006). Mechanical properties and durability of cement mortar containing dry sludge ash from Bang Khen water supply plant. **In Proceedings of National Convention on Civil Engineering 2006 (NCCE11)**. 20-22 April 2006, Phuket.
- Holmbee, M., Wold, S. and Petterson, T. (2011). Effects of the injection grout silica sol on bentonite. **Physics and Chemistry of the Earth**. 36: 1580-1589.
- Hong, C. S., Shackelford, C. D. and Malusis, M. A. (2012). Consolidation and Hydraulic Conductivity of Zeolite-Amended Soil-Bentonite Backfills. **Geotech. Geoenviron. Eng.** 138(1): 15–25.
- Huang, W. H. (1997). Properties of cement-fly ash grout admixed with bentonite, silica fume, or organic fiber. **Cement and Concrete Research**. 27(3): 395-406.
- Huang, Z., Chen, M. and Chen, X. (2003). A developed technology for wet-ground fine cement slurry with its applications. **Cement and Concrete Research**. 33: 729-732.
- Hvorlsev, M. S. (1951). Time lag and soil permeability in groundwater measurements. U.S. Corps of Engineers Waterways Experiment Station, **Bulletin No. 36**, 50p.
- IAEA (1990). Sealing of underground repositories for radioactive wastes. In Gray, M., Gera, F., Wiley, J.R., Dlouhy, Z., Squires, D. (Eds.). **Technical Reports Series No. 319**. International Atomic Energy Agency, Vienna, Unipub, Lanham, MD.
- Indraratna, B. and Ranjith, P. (2001). **Hydromechanical aspects and unsaturated flow in joints rock**. A. A. Balkema, Lisse, 83-154.

- Jaeger, J. C., and Cook, N. G. W. (1979). **Fundamentals of Rock Mechanics (3rd ed.)**. London: Chapman & Hall.
- Jaeger, J.C. (1959). The frictional properties of joints in rocks. **Geofis pura appl.** 43: 148-158.
- Jones, F. O. (1975). A laboratory study of the effects of confining pressure on fracture flow and storage capacity in carbonate rocks. **Journal of Petroleum Technology.** 21: 21-27.
- Joshi, K., Kechavarzi, C., Sutherland, K., Albert, M. Y. Soga, K. and Tedd, P. (2010). Laboratory and in situ tests for long-term hydraulic conductivity of a cement-bentonite cutoff wall. **J. Geotech. Geoenviron. Eng.** 136(4): 562-572.
- Kjartanson, B.H., Chandler, N.A. and Wan, A.W.L. (1996). In situ performance of a clay based barrier. In Fuenkajorn, K., Daemen, J.J.K. (Eds.), **Sealing of Boreholes and Underground Excavations in Rock**. Chapman and Hall, London, pp. 96–125.
- Koch, D. (2002). Bentonites as a basic material for technical base liners and site encapsulation cut-off walls. **Applied Clay Science.** 21: 1-11
- Komine, H., (2004). Simplified evaluation on hydraulic conductivities of sand–bentonite mixture backfill. **Applied Clay Science.** 26: 13–19.
- Laothong, K. (2003). **The Utilization of Sludge Cake from Water Treatment Processes of Wang Noi Power Plant. Master of Engineering (Environmental Engineering)**. Major Field Environmental Engineering, Department of Environmental Engineering, Kasetsart University, 99 pp.

- Lee, J.-M. and Shackelford, C. D. (2005). Impact of bentonite quality on hydraulic conductivity of geosynthetic clay liners. **Journal of Geotechnical and Geoenvironmental Engineering**. 131(1): 64-77.
- Malusis, M. A., Barben, E. J. and Evans, J. C. (2009). Hydraulic conductivity and compressibility of soil-bentonite backfill amended with activated carbon. **J. Geotech. Geoenviron. Eng.** 135(5): 664–672.
- Metcalf, R. and Walker, C. (2004). **International Workshop on Bentonite Cement Interaction in Repository Environments**. NUMO Technical Report.
- Navarro, F. C. (2010). Suggested guidelines for sampling natural stones for laboratorial tests. **Global Stone Congress**. (pp. 1-5).
- Nelson, R. (1975). Fracture Permeability in Porous Reservoirs: Experimental and Field Approach. **Ph.D. Thesis**. Texas A&M University.
- Nimjaroen, C (2013). Porous glass from coal fly ash preparation, characterization and its adsorption study. **Ph.D. Thesis**. Suranaree University of Technology
- Obcheoy, J., Aracheeploha, S. and Fuenkajorn, K. (2011). Fracture permeability under normal and shear stresses. Rock Mechanics, Fuenkajorn & Phien-wej (eds), **In Proceedings of the Third Thailand Symposium on Rock Mechanics**. March, 10-11, Cha-Am, Thailand, Published by Geomechanics Research Unit, Suranaree University of Technology, Nakhon Ratchasima, Thailand, pp. 133-140.
- Owaidat, L. M., Andromalos, K. B., and Sisley, J. L. (1999). Construction of a soil-cement-bentonite slurry wall for a levee strengthening program. **In Association of State Dam Safety Officials Annual Conference**. 10-12 October 1999, St. Louis, Missouri.

- Poonsawat, C. and Lertpocasombut, K. (2006). Study on the properties of sludge from water supply plant as raw material for clay plan roofing tile. **In National Convention on Civil Engineering (NCCE11)**. 20-22 April 2006, Phuket.
- Pusch, R. (1983). Borehole sealing for underground waste storage. **ASCE Journal of Geotechnical Engineering**. 109: 113-119.
- Pusch, R. (1994). Waste disposal in rock. **Developments in Geotechnical Engineering**. pp.76, Elsevier, Amsterdam.
- Rahmani, H. (2004). Estimation of grout distribution in a fractured rock by numerical modeling. **M.S. Thesis**. University of Tehran.
- Ranjith, P. G. and Viete, D. R. (2011). Applicability of the 'cubic law' for non-Darcian fracture flow. **Petroleum Science and Engineering**. In Press, Accepted Manuscript, Available online 7 August 2011.
- Rutqvist, J. (1995). Determination of Hydraulic Normal Stiffness of Fractures in Hard Rock from Well Testing. **Rock Mech. Min. Sci. & Geomech.** 32(5): 513-523.
- Ryan, C. R., and Day, S. R. (2002). Soil-Cement-Bentonite Slurry Wall. **International Deep Foundation Congress**. GSP No. 116, American Society of Civil Engineers, Orlando, FL.
- Saiyouri, N., Bouasker, M. and Khelidj, A. (2008). Gas permeability measurement on injected soils with cement grout. **Cement and Concrete Research**. 38: 95-103.
- Sa-ngiumsak, N. and Cheerarot, R. (2008). The study of properties of artificial aggregates made from water supply sludge. **In National Convention on Civil Engineering (NCCE11)**. 14-16 Mayl 2008, Pattaya, Chonburi.
- Snow, D. T. (1968). Anisotropic Permeability of Fractured Media. **Water Resources Research**. 5(6): 1273-1289.

- Sonsakul, P., Fuenkajorn, K. (2013). Envelopment of three-ring compaction and direct shear test mold for soils with oversized particles. **Research and Development Journal of The Engineering institute of Thailand**. 24(2): 1-7.
- Suanprom, P. Obcheoy, J. and Fuenkajorn, K. (2009). Permeability of rock fractures under shear stresses. **EIT-JSCE Joint International Symposium Geotechnical Infrastructure Asset Management**. Bangkok, Thailand.
- Svermova, L. Sonebi, M. and Barto, P. J. M. (2003). Influence of mix proportions on rheology of cement grouts containing limestone powder. **Cement & Concrete Composites**. 25:737-749.
- Svermova, L., Sonebi, M., Bartos, P.J.M. (2003). Influence of mix proportions on rheology of cement grouts containing limestone powder. **Cement & Concrete Composites**. 25, 737-749.
- Tepnarong, P. (2012). Bond strength of cement sealing in Maha Sarakham salt. **Proc. of 7th Asian Rock Mechanics Symposium**. Seoul, Korea, 15-19 October 2012, 584-593.
- Tepnarong, P. and Deethouw, P. (2014). Mechanical and hydraulic performance of sludge-mixed cement borehole plugs in rock salt. **Proc. of 8th Asian Rock**.
- Tepnarong, P. and Pattani, S. (2015). Experimental assessment of mechanical and hydraulic performance of cement sealing in rock salt. **ISRM VietRock International Workshop**. 12-13 March, Hanoi, Vietnam.
- Terzaghi, K. (1936). The Shearing Resistance of Saturated Soils. **In Proceedings of the International Conference on Foundation Engineering**. Graduate School of Engineering, pp.402-407, Harvard University. Boston: Spaulding Moss.

- Trakoolngam, K. (2009). Determination of the mechanical-hydraulic coupled behavior of the Phu Thok sandstone: A dual-porosity approach. **In Proceedings of the Second Thailand Symposium on Rock Mechanics.** March 12-13, 2009, Chonburi, Published by Geomechanics Research Unit, Suranaree University of Technology, Nakhon Ratchasima, Thailand (pp. 219-234).
- Tsang, Y. W. (1992). Usage of equivalent apertures for rock fractures as derived from hydraulic and tracer tests. **J. Water Resource.** Res. 28(5): 1451-1455.
- USEPA. (1995). **Environmental radiation protection standards for management and disposal of spent nuclear fuel, high-level and transuranic radioactive wastes.** CFR 40, Part 191, Washington, D.C.
- Varol, A., and Dalgic, S. (2006). Grouting applications in the Istanbul metro, **Turkey. Tunneling and Underground Space Technology.** 21: 602-612
- Vitipanit, S. and Rianbupa, S. (2004). A study for development an appropriate material in construction by using sand mixed with bentonite. **Research and Development Institute.** Royal Irrigation Department.
- Wetchasat and Fuenkajorn, (2012) Laboratory assessment of mechanical and hydraulic performance of sludge-mixed cement grout in rock fractures. **Proceedings of the Third Thailand Symposium On Rock Mechanics.** pp 143- 152.
- Witherspoon, P. A., Wang, J. S. Y., Iwai, K. and Gale, J. E. (1980). Validity of cubic law for fluid flow in a deformable rock fracture. **Water Resource.** Res. 16(6): 1016-1024.
- Yan, S., Sagoe-Crentsil, K. and Shapiro, G. (2011). Reuse of de-inking sludge from wastepaper recycling in cement mortar products. **Journal of Environmental Management.** 92: 2085-2090.

BIOGRAPHY

Mr. Monton Chiangmai was born on April 22, 1991 in Nakhon Ratchasima province, in Thailand. He received his Bachelor's Degree in Engineering (Geotechnology) from Suranaree University of Technology in 2013. For his post-graduate, he continued to study with a Master's degree in the Geological Engineering Program, Institute of Engineering, Suranaree university of Technology. During graduation, 2014-2016, he was a part time worker in position of research assistant at the Geomechanics Research Unit, Institute of Engineering, Suranaree University of Technology.

